Received: 14 December 2021 | Revised: 15 April 2023 | Accepted: 17 April 2023

DOI: 10.1002/nme.7256

RESEARCH ARTICLE

WILEY

A partitioned combined computational method for multi-scale dynamic systems

Peng Yuan[1] | **Sondipon Adhikari**[2] | **You Dong**[1]

[1]Department of Civil and Environmental Engineering, The Hong Kong Polytechnic University, Hong Kong, China

[2]James Watt School of Engineering, University of Glasgow, Glasgow, UK

Correspondence
You Dong, Department of Civil and Environmental Engineering, The Hong Kong Polytechnic University, Hong Kong 999077, China.
Email: you.dong@polyu.edu.hk

Funding information
Research Grant Council of Hong Kong, Grant/Award Number: 15219819; The HOng Kong Polytechnic University—Postdoc Matching Fund Scheme; the Young Scientists Fund of the National Natural Science Foundation of China, Grant/Award Number: 52208212

Abstract

A partitioned/combined computational method based on Newmark scheme is proposed to analyze dynamic systems with different temporal scales and element scales. To effectively filter spurious high-frequency vibration content and retain the second-order accuracy simultaneously, Generalized-α schemes are investigated and incorporated into the proposed method. The proposed method can decompose a complete domain into several independent computational subdomains (≥3), and several independent substructures can be combined into a complete computational structure. The accuracy and stability of responses in different subdomains can be ensured and adjusted by using their own integration parameters and time-step sizes. The energy conservation property is preserved in the proposed method. Only one calculation is performed at each time step for all subdomains, and computational information exchange between subdomains is only conducted at the system time step, therefore, the computational efficiency is improved significantly compared with the existing multi-time-step methods. The derivation process and theoretical demonstration of the proposed method are given in detail. Two representative examples, namely, a single degree of freedom system split into four subdomains and a sandwich beam subjected to high-frequency impact loads, are studied to systematically demonstrate the proposed method's accuracy, energy properties, and efficiency compared with the existing multi-time-step methods.

KEYWORDS

desirable algorithmic damping, energy conservation, multiple temporal and element scales, partitioned/combined computation, stability and accuracy

1 | INTRODUCTION

As the complexity of practical engineering problems increases significantly, how to simultaneously utilize the high efficiency of explicit integration methods and the potential unconditional stability of implicit integration methods[1,2] to solve complex dynamic problems has been a topic of great interest. Partitioned computational methods considering explicit/implicit hybrid schemes have been extensively researched to efficiently and accurately calculate responses of complex dynamic systems.[3]

Three partitioned computational methods were developed to solve complex dynamic systems: the mixed methods,[4] the multi-time-step methods,[5] and the mixed-multi-time-step methods.[6] The mixed methods (explicit and implicit)[7]

considering a unique time step were proposed based on nodal or element partitioning. The multi-time-step methods (also called sub-cycling)[5] were then developed. Specifically, by using multi-time-step methods, a domain is partitioned into multiple subdomains that are updated with different time steps. However, proof of stability is available only for some particular integration schemes,[8] or possible numerical dissipation occurs at the interfaces connected with different subdomains. After Farhat and Roux developed the finite element tearing and interconnecting (FETI) method,[9–11] the mixed-multi-time-step methods (MMTS) were proposed. Using the FETI method, a complex or large-scale structure can be divided into different subdomains with non-overlapping elements,[6] that is, subdomains are interconnected by interface nodes. Recently, by imposing velocity continuity conditions on the interfaces of shared nodes, Gravouil and Combescure (GC method) proposed[12] and improved MMTS methods[13–17] to couple arbitrary Newmark schemes. However, energy conservation can only be retained when all subdomains have a unique time step. To address this issue, Prakash and Hjelmstad[16,18,19] (PH) proposed an algorithm with the energy conservation property. Moreover, two new coupling methods, that is, BGC-micro and BGC-macro,[20,21] were developed to couple the Newmark scheme and HHT-α scheme in a linear dynamic system. The BGC-micro and BGC-macro methods considering Newmark scheme exactly match GC[12] and PH,[16] respectively.

Despite numerous works investigated before, further developments towards efficient coupling computational methods are necessary for higher dimensional problems. The main reasons include:

1. The border programme with complex time-consuming storage must be employed in the existing MMTS methods to obtain responses of a coupling system; each subdomain vibration is divided into free vibrations and link vibrations; and loads are also split into external excitations and link forces.[20,21] Namely, the computational efficiency of existing MMTS methods could be improved significantly. More information on the border programme and the computational procedure of MMTS can be accessed in References 20,21.
2. To extend the application of MMTS methods to the system with multiple subdomains (≥3), the complex recursive coupling approaches[22–24] have to be employed to couple all subdomains simultaneously, which leads to some new complex issues, such as searching for an optimal mesh decomposition.[23] Namely, it is not easy to extend the application of MMTS methods to the system with multiple subdomains (≥3) by using existing methods.[25]

To directly address these major drawbacks of the existing methods, i.e., low computational efficiency, limitation of the number of subdomains (usually two), and energy dissipation, we propose a partitioned/combined computational method. The main aims are: (a) to improve the computational efficiency; (b) to overcome the limitation on the number of computational subdomains; and (c) to ensure the conservation of system energy and high accuracy. To clearly illustrate the proposed method, the remainder of this study is organized as follows. In Section 2, the interface-based coupling dynamic equations and the compact form of dynamic equations considering Newmark method are derived to solve the coupling subdomains with different element scales and temporal scales, respectively. In Section 3, using the velocity continuity condition and the velocity increment within the system time step, interface link forces are solved to decouple the system into independent subdomains. In Section 4, the energy conservation property is investigated to discuss the stability of the proposed method. In Section 5, to filter high-frequency spurious vibrations and ensure accuracy of responses in the low-frequency simultaneously, Generalized-α integration schemes (NG)[18,26] with desirable algorithmic damping are studied and incorporated into the proposed method. It is worth noting that the energy stability derivation is only performed for the proposed method with Newmark scheme in Sections 2, 3, and 4. In Section 6, two representative examples are employed to demonstrate the accuracy, efficiency, and energy dissipation of the proposed method. Finally, the main conclusions from this study are drawn in Section 7.

2 | ESTABLISHMENT OF A MULTI-SCALE DYNAMIC SYSTEM

2.1 | Interface-based dynamic equations with different element-scales

According to the frequency content and boundary conditions of the problem, the complete computational domain Ω shown in Figure 1A is divided into S non-overlapping subdomains (i.e., subdomains are interconnected by interface nodes, as shown in Figure 1B).[9–11] The interconnected subdomains would be used to discuss the partitioned calculation method.[27] Similarly, S independent substructures[28–30] (see Figure 1C) are combined into an entire computational domain, as shown in Figure 1A. The independent substructures would be used to discuss the combined calculation

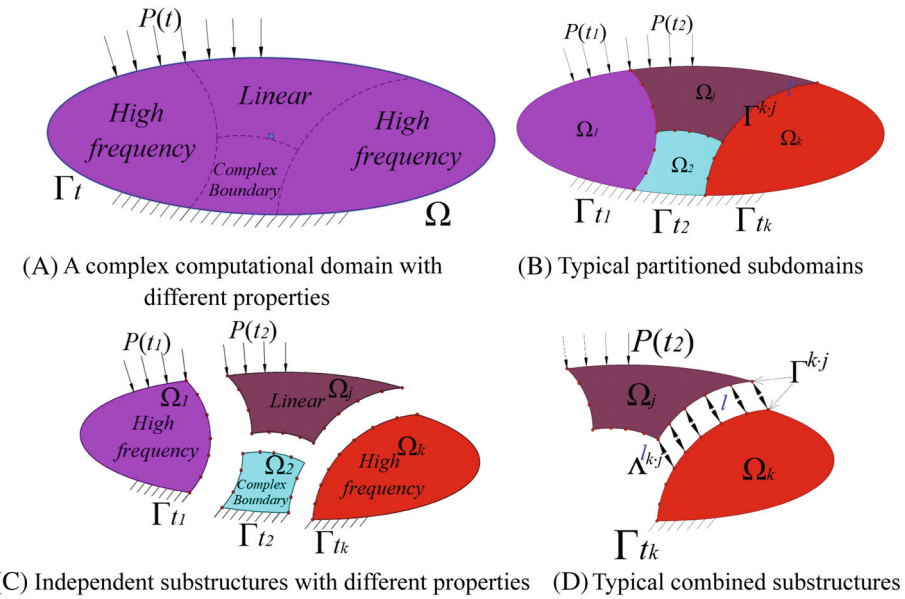

FIGURE 1 A partitioned/combined computational problem. Γ_t is boundary condition, and $\mathbf{\Lambda}^{l_{k\cdot j}}$ and $\mathbf{\Gamma}^{k\bullet j}$ are the link force and the l interface of the kth and jth subdomains, respectively

method. Interconnected subdomains/substructures (e.g., Ω_k and Ω_j) have shared nodes at the interface $\mathbf{\Gamma}^{k\bullet j}$, as marked in Figures 1B,D, created by partitioning/combining. Each subdomain/substructure is interconnected with multiple subdomains/substructures by link forces $\mathbf{\Lambda}^{l_{k\cdot j}}$ (see Figure 1D). Where the superscripts k, j, and l indicate two subdomain numbers and an interface number.

Hamilton's principle is used to build coupling dynamic equations of subdomains with different element sizes (called the element scale). Taking the kth subdomain for example, the difference between the kinetic energy and potential energy for the system Ω is:

$$\zeta = \sum_{k=1}^{S} \left(\frac{1}{2} \boldsymbol{v}^{k^T} \boldsymbol{M}^k \boldsymbol{v}^k - \frac{1}{2} \boldsymbol{u}^{k^T} \boldsymbol{K}^k \boldsymbol{u}^k \right) \tag{1}$$

where $\boldsymbol{M}^k$, $\boldsymbol{K}^k$, $\boldsymbol{u}^k$, and $\boldsymbol{v}^k$ are the mass matrix, stiffness matrix, displacement vector, and velocity vector of the kth subdomain, respectively; and the letter $\square^T$ indicates the matrix/vector transpose operation such as $\boldsymbol{u}^{k^T}$ and $\boldsymbol{v}^{k^T}$. Note that the calculation time point of all quantities in Equation (1) is set at the same time step such as t_{n+1}, and scripts related to time are thus temporarily ignored for simplification. The virtual work generated by non-conservation forces (i.e., external excitations and damping forces) is calculated as:

$$\delta\varkappa = \sum_{k=1}^{S} \delta \boldsymbol{u}^{k^T} \left(\boldsymbol{P}^k - \boldsymbol{C}^k \boldsymbol{v}^k \right) \tag{2}$$

where $\boldsymbol{P}^k$ and $\boldsymbol{C}^k$ are the given external excitations and damping matrices of the kth subdomain, respectively. The velocity continuity conditions are selected to be imposed on all interfaces.[14,15] For instance, the continuity condition at the l interface, connecting to the kth subdomain and the jth subdomain (see Figure 1B), is written as follows:

$$\boldsymbol{L}_l^{k\cdot j} \boldsymbol{v}^k + \boldsymbol{L}_l^{j\cdot k} \boldsymbol{v}^j = 0 \tag{3}$$

where $\boldsymbol{L}_l^{k\cdot j}$ is Boolean matrix; the superscripts refer to two subdomain numbers (Note the order of the letters); and the subscript is the interface number. The matrix has $L \times N_{k\bullet j}$ dimensions, where $N_{k\bullet j}$ indicates the number of degrees of freedom (DOF) of the kth subdomain and L represents the number of DOF of the l interface connected with the jth subdomain (i.e., a new boundary condition $\mathbf{\Gamma}^{k\bullet j}$ as shown in Figure 1D). Further information on the Boolean matrix can

be found in Reference 16. Based on the obtained system kinetic energy, potential energy, and virtual work, Hamilton equation augmented with velocity continuity conditions are:

$$\int_{t_1}^{t_2}\left(\delta\zeta+\delta\varkappa+\delta\sum_{k=1}^{S}\left(\sum_{l=1}^{S_k}\lambda_l^{k\cdot j^T}\left(\boldsymbol{L}_l^{k\cdot j}\boldsymbol{v}^k+\boldsymbol{L}_l^{j\cdot k}\boldsymbol{v}^j\right)\right)\right)dt=0 \tag{4}$$

where $\lambda_l^{k\cdot j}$ is a Lagrange multiplier of the kth subdomain at the l interface,[31] and S_k refers to the number of interfaces of the kth subdomain (i.e., S_k subdomains interconnect with the kth subdomain). Substituting Equations (1) and (2) into Equation (4), the total energy of the domain Ω is obtained as follows:

$$\int_{t_1}^{t_2}\sum_{k=1}^{S}\left(\begin{array}{c}\left(\delta\boldsymbol{v}^{k^T}\boldsymbol{M}^k\boldsymbol{v}^k-\delta\boldsymbol{u}^{k^T}\boldsymbol{K}^k\boldsymbol{u}^k\right)+\delta\boldsymbol{u}^{k^T}\left(\boldsymbol{P}^k-\boldsymbol{C}^k\boldsymbol{v}^k\right)+\\ \sum_{l=1}^{S_k}\delta\lambda_l^{k\cdot j^T}\left(\boldsymbol{L}_l^{k\cdot j}\boldsymbol{v}^k+\boldsymbol{L}_l^{j\cdot k}\boldsymbol{v}^j\right)+\sum_{l=1}^{S_k}\left(\lambda_l^{k\cdot j^T}\boldsymbol{L}_l^{k\cdot j}\delta\boldsymbol{v}^k+\lambda_l^{k\cdot j^T}\boldsymbol{L}_l^{j\cdot k}\delta\boldsymbol{v}^j\right)\end{array}\right)dt=0 \tag{5a}$$

The total energy can be written as:

$$\int_{t_1}^{t_2}\sum_{j=1}^{S}\left(\begin{array}{c}\left(\delta\boldsymbol{v}^{j^T}\boldsymbol{M}^j\boldsymbol{v}^j-\delta\boldsymbol{u}^{j^T}\boldsymbol{K}^j\boldsymbol{u}^j\right)+\delta\boldsymbol{u}^{j^T}\left(\boldsymbol{P}^j-\boldsymbol{C}^j\boldsymbol{v}^j\right)+\\ \sum_{l=1}^{S_j}\delta\lambda_l^{j\cdot k^T}\left(\boldsymbol{L}_l^{j\cdot k}\boldsymbol{v}^j+\boldsymbol{L}_l^{k\cdot j}\boldsymbol{v}^k\right)+\sum_{l=1}^{S_j}\left(\lambda_l^{j\cdot k^T}\boldsymbol{L}_l^{j\cdot k}\delta\boldsymbol{v}^j+\lambda_l^{j\cdot k^T}\boldsymbol{L}_l^{k\cdot j}\delta\boldsymbol{v}^k\right)\end{array}\right)dt=0 \tag{5b}$$

According to the virtual work principle, the last element at Equation (5a) can be exchanged with the last element at Equation (5b). The updated total energy of the system is:

$$\int_{t_1}^{t_2}\sum_{k=1}^{S}\left(\begin{array}{c}\left(\delta\boldsymbol{v}^{k^T}\boldsymbol{M}^k\boldsymbol{v}^k-\delta\boldsymbol{u}^{k^T}\boldsymbol{K}^k\boldsymbol{u}^k\right)+\delta\boldsymbol{u}^{k^T}\left(\boldsymbol{P}^k-\boldsymbol{C}^k\boldsymbol{v}^k\right)+\\ \sum_{l=1}^{S_k}\delta\lambda_l^{k\cdot j^T}\left(\boldsymbol{L}_l^{k\cdot j}\boldsymbol{v}^k+\boldsymbol{L}_l^{j\cdot k}\boldsymbol{v}^j\right)+\sum_{l=1}^{S_k}\left(\lambda_l^{k\cdot j^T}\boldsymbol{L}_l^{k\cdot j}\delta\boldsymbol{v}^k+\lambda_l^{j\cdot k^T}\boldsymbol{L}_l^{k\cdot j}\delta\boldsymbol{v}^k\right)\end{array}\right)dt=0 \tag{6}$$

Replacing $\lambda_l^{k\cdot j^T}+\lambda_l^{j\cdot k^T}$ by $\bar{\lambda}_l^{k\cdot j^T}$ and rearranging Equation (6), one has:

$$\int_{t_1}^{t_2}\sum_{k=1}^{S}\left(\begin{array}{c}\delta\boldsymbol{v}^{k^T}\left(\boldsymbol{M}^k\boldsymbol{v}^k+\sum_{l=1}^{S_k}\boldsymbol{L}_l^{k_j^T}\bar{\lambda}_l^{k\cdot j}\right)+\\ \delta\boldsymbol{u}^{k^T}\left(\boldsymbol{P}^k-\boldsymbol{C}^k\boldsymbol{v}^k-\boldsymbol{K}^k\boldsymbol{u}^k\right)+\sum_{l=1}^{S_k}\delta\lambda_l^{k\cdot j^T}\left(\boldsymbol{L}_l^{k\cdot j}\boldsymbol{v}^k+\boldsymbol{L}_l^{j\cdot k}\boldsymbol{v}^j\right)\end{array}\right)dt=0 \tag{7}$$

The displacement and velocity at the virtual times t_1 and t_2 satisfy: $\delta\boldsymbol{u}_{t_1}^k=\delta\boldsymbol{u}_{t_2}^k=0$ and $\delta\boldsymbol{v}_{t_1}^k=\delta\boldsymbol{v}_{t_2}^k=0$. Integrating the first element of Equation (7) and rearranging it, one gets:

$$\int_{t_1}^{t_2}\left(\sum_{k=1}^{S}\left[\begin{array}{c}\delta\boldsymbol{u}^{k^T}\left(\boldsymbol{M}^k\boldsymbol{a}^k+\boldsymbol{C}^k\boldsymbol{v}^k+\boldsymbol{K}^k\boldsymbol{u}^k+\sum_{l=1}^{S_k}\boldsymbol{L}_l^{k\cdot j^T}\bar{\lambda}_l^{k\cdot j}-\boldsymbol{P}^k\right)\\ -\sum_{l=1}^{S_k}\delta\lambda_l^{k\cdot j^T}\left(\boldsymbol{L}_l^{k\cdot j}\boldsymbol{v}^k+\boldsymbol{L}_l^{j\cdot k}\boldsymbol{v}^j\right)\end{array}\right]\right)dt \tag{8}$$

According to the principle of the variations calculus and replacing the variable $\bar{\lambda}_l^{k\cdot j}$ by $\boldsymbol{\Lambda}^{l_{k\cdot j}}$ (i.e., the link force at the l interface, as marked in Figure 1D), the interface-based dynamic equations are derived as follows:

$$\boldsymbol{M}^k\boldsymbol{a}^k+\boldsymbol{C}^k\boldsymbol{v}^k+\boldsymbol{K}^k\boldsymbol{u}^k+\sum_{l=1}^{S_k}\boldsymbol{L}_l^{k\cdot j^T}\boldsymbol{\Lambda}^{l_{k\cdot j}}=\boldsymbol{P}^k\qquad k=\{1,\cdots S\} \tag{9}$$

For the kth subdomain with S_k interfaces (i.e., with j interconnected subdomains), the velocity continuity conditions are:

$$\boldsymbol{L}_l^{k\cdot j}\boldsymbol{v}^k+\boldsymbol{L}_l^{j\cdot k}\boldsymbol{v}^j=0\qquad(l,j)=\{1,\cdots S_k\} \tag{10}$$

So far, interface-based coupling dynamic Equation (9) for subdomains with different element scales have been established.

2.2 | Compact form of dynamic equations with different temporal-scales

Due to the introduction of the temporal scale in this sub-section, subscripts related to time are added to variables for interpretation, with the notation $\square_{t_i}^{l_{k\bullet j}}$. Its subscript t_i refers to the time step number (called the temporal scale), and its superscript $l_{k\bullet j}$ indicates an interface number (l) and two subdomain numbers (k and j). Note that the interface number l is marked only for the link force. The dynamic equations of subdomains with different temporal scales are here built using the Newmark scheme since it has a strict energy stability demonstration.[32] Incremental expressions of the displacement and velocity for the kth subdomain are:

$$\Delta \boldsymbol{u}_{t_{i+1}}^{k} = \frac{\beta^k \Delta h^k}{\gamma^k} \Delta \boldsymbol{v}_{t_{i+1}}^{k} + \Delta h^k \boldsymbol{v}_{t_i}^{k} + \frac{\gamma^k - 2\beta^k}{2\gamma^k} \Delta h^{k^2} \boldsymbol{a}_{t_i}^{k} \tag{11a}$$

$$\Delta \boldsymbol{a}_{t_{i+1}}^{k} = \frac{1}{\gamma^k \Delta h^k} \Delta \boldsymbol{v}_{t_{i+1}}^{k} - \frac{1}{\gamma^k} \boldsymbol{a}_{t_i}^{k} \tag{11b}$$

where subscript t_i and t_{i+1} represent two time-step numbers; Δh^k implies the time-step size; the algorithmic parameters γ^k and β^k are adopted to adjust the accuracy and stability of Newmark schemes; and Δ denotes the increment of kinematic quantities at each time-step size such as $\Delta \boldsymbol{u}_{t_{i+1}}^{k} = \boldsymbol{u}_{t_{i+1}}^{k} - \boldsymbol{u}_{t_i}^{k}$. It is worth noting that a subdomain can connect with multiple subdomains, but an interface can and only can have two interconnected subdomains (see Figure 1). Two interconnected subdomains with different temporal scales, as shown in Figure 2, are employed to illustrate the derivation process of the compact form of dynamic equations with different temporal scales.

Substituting Equation (11) into the interface-based dynamic equations without damping (i.e., Equation (9)), the incremental form of the dynamic Equation (9) for the kth subdomain is derived as:

$$\boldsymbol{K}^{*k} \Delta \boldsymbol{v}_{t_{i+1}}^{k} + \sum_{l=1}^{S_k} \boldsymbol{L}_{l}^{k\cdot j^T} \Delta \boldsymbol{\Lambda}_{t_{i+1}}^{l_{k\cdot j}} = \Delta \boldsymbol{F}_{t_{i+1}}^{k} \tag{12a}$$

$$\boldsymbol{K}^{*k} = \frac{1}{\gamma^k \Delta h^k} \boldsymbol{M}^k + \frac{\beta^k \Delta h^k}{\gamma^k} \boldsymbol{K}^k \tag{12b}$$

$$\Delta \boldsymbol{F}_{t_{i+1}}^{k} = \Delta \boldsymbol{P}_{t_{i+1}}^{k} - \boldsymbol{K}^k \left(\frac{\gamma^k - 2\beta^k}{2\gamma^k} \Delta h^{k^2} \boldsymbol{a}_{t_{i+1}}^{k} + \Delta h^k \boldsymbol{v}_{t_{i+1}}^{k} \right) + \frac{1}{\gamma^k} \boldsymbol{M}^k \boldsymbol{a}_{t_{i+1}}^{k} \tag{12c}$$

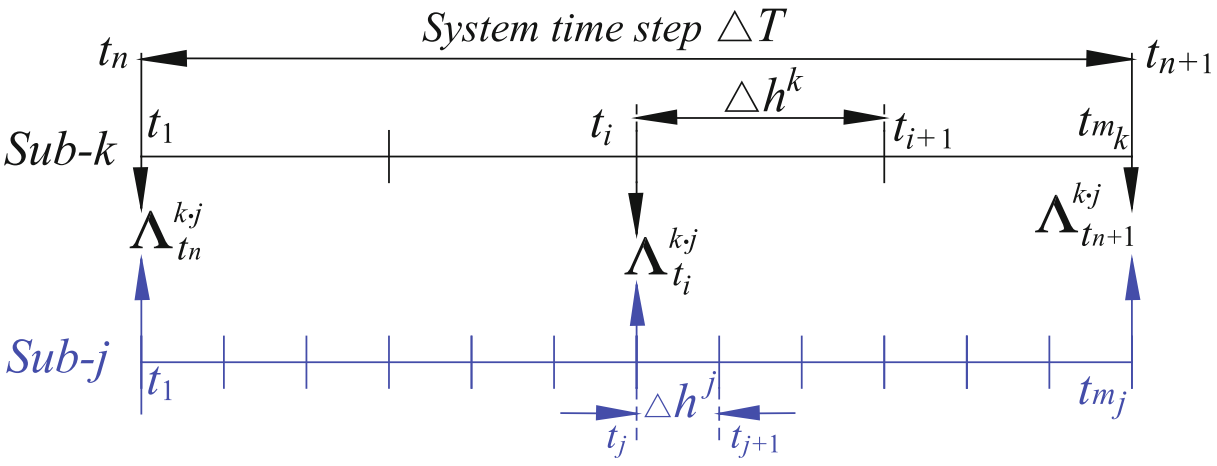

FIGURE 2 Two typical interconnected subdomains with different time sub-steps. Note that ΔT is the system time-step size; Δh^k and m_k refer to the time step size and the number of the time sub-step, respectively[33]; and $\boldsymbol{\Lambda}_{t_n}^{k\cdot j}$ and $\boldsymbol{\Lambda}_{t_{n+1}}^{k\cdot j}$ indicate the link forces at the beginning t_n and end t_{n+1} time step, respectively (see Figure 1D)

For simplification, Equations (11) and (12) are rewritten in a compact form as follows:

$$\mathbb{K}^{*k}\Delta\mathbb{U}^k_{t_{i+1}} + \mathbb{L}^T_k\Delta\mathfrak{R}^k_{t_{i+1}} = \Delta\mathbb{P}^k_{t_{i+1}} - \mathbb{N}^k\mathbb{U}^k_{t_{i+1}} \tag{13a}$$

$$\mathbb{K}^{*k} = \begin{bmatrix} \boldsymbol{I}^k & -\frac{\beta^k\Delta h^k}{\gamma^k}\boldsymbol{I}^k & 0 \\ 0 & \boldsymbol{K}^k_* & 0 \\ 0 & -\frac{1}{\gamma^k\Delta h^k}\boldsymbol{I}^k & \boldsymbol{I}^k \end{bmatrix} \Delta\mathbb{U}^k_{t_{i+1}} = \begin{bmatrix} \Delta\boldsymbol{u}^k_{t_{i+1}} \\ \Delta\boldsymbol{v}^k_{t_{i+1}} \\ \Delta\boldsymbol{a}^k_{t_{i+1}} \end{bmatrix} \mathbb{U}^k_{t_{i+1}} = \begin{bmatrix} \boldsymbol{u}^k_{t_{i+1}} \\ \boldsymbol{v}^k_{t_{i+1}} \\ \boldsymbol{a}^k_{t_{i+1}} \end{bmatrix} \Delta\mathbb{P}^k_{t_{i+1}} = \begin{bmatrix} 0 \\ \Delta\boldsymbol{P}^k_{t_{i+1}} \\ 0 \end{bmatrix}. \tag{13b}$$

$$\mathbb{N}^k = \begin{bmatrix} 0 & -\Delta h^k\boldsymbol{I}^k & -\frac{\gamma^k-2\beta^k}{2\gamma^k}\Delta h^{k^2}\boldsymbol{I}^k \\ 0 & \Delta h^k\boldsymbol{K}^k & \frac{\gamma^k-2\beta^k}{2\gamma^k}\Delta h^{k^2}\boldsymbol{K}^k - \frac{1}{\gamma^k}\boldsymbol{M}^k \\ 0 & 0 & \frac{1}{\gamma^k}\boldsymbol{I}^k \end{bmatrix} \mathbb{L}^T_k = \begin{bmatrix} \boldsymbol{L}^{k_1^T}_1 \\ \boldsymbol{L}^{k_2^T}_2 \\ \vdots \\ \boldsymbol{L}^{k_{Sk}^T}_{S_k} \end{bmatrix}^T \Delta\mathfrak{R}^k_{t_{i+1}} = \begin{bmatrix} \Delta\boldsymbol{\Lambda}^{1_{k1}}_{t_{i+1}} \\ \Delta\boldsymbol{\Lambda}^{2_{k2}}_{t_{i+1}} \\ \vdots \\ \Delta\boldsymbol{\Lambda}^{S_{k_kS_k}}_{t_{i+1}} \end{bmatrix}. \tag{13c}$$

Using Equations (9) and (13), coupling equations of S subdomains are derived as follows:

$$\begin{cases} \mathbb{K}^{*1}\Delta\mathbb{U}^1_{t_i} + \mathbb{L}^T_1\Delta\mathfrak{R}^1_{t_i} = \mathbb{F}^1_{t_i} & \forall t_i \in \{1, m_i\} \\ \vdots & \vdots \\ \mathbb{K}^{*k}\Delta\mathbb{U}^k_{t_k} + \mathbb{L}^T_k\Delta\mathfrak{R}^k_{t_k} = \mathbb{F}^k_{t_k} & \forall t_k \in \{1, m_k\} \\ \vdots & \vdots \\ \mathbb{K}^{*S}\Delta\mathbb{U}^S_{t_S} + \mathbb{L}^T_S\Delta\mathfrak{R}^k_{t_S} = \mathbb{F}^S_{t_S} & \forall t_S \in \{1, m_S\} \end{cases} \tag{14a}$$

$$\Delta\mathfrak{R}^k_{t_k} = \begin{bmatrix} \Delta\boldsymbol{\Lambda}^{1_{k\cdot1}}_{t_k} & \Delta\boldsymbol{\Lambda}^{2_{k\cdot2}}_{t_k} & \cdots & \Delta\boldsymbol{\Lambda}^{S_{k_{k\cdot S_k}}}_{t_k} \end{bmatrix}^T \tag{14b}$$

where $m_k = \Delta T/\Delta h^k$ is the number of the time sub-steps of the kth subdomain within ΔT, from the beginning time point t_1 to the ending time point t_{m_k} (see Figure 2). Each subdomain is connected to S_k subdomains by S_k interfaces, and the whole domain has $\tilde{S}$ interfaces $\left(\tilde{S} = \frac{1}{2}\sum_{k=1}^{S} S_k\right)$. The velocity continuity condition built at the system time step t_{n+1} is:

$$\boldsymbol{L}^{k\cdot j}_l\boldsymbol{v}^k_{t_{n+1}} + \boldsymbol{L}^{j\cdot k}_l\boldsymbol{v}^j_{t_{n+1}} = 0 \qquad l = \{1, \cdots \tilde{S}\} \tag{15}$$

Although the velocity continuity conditions provide $\tilde{S}$ supplementary equations for solving Equation (14), the link forces (e.g., $\Delta\boldsymbol{\Lambda}^{l_{k\cdot j}}_{t_i}$ at Equation (14b), as shown in Figure 2) within the system time steps still cannot be calculated. Therefore, to simplify the calculation of the link forces within ΔT, a linear interpolation is adopted as follows:

$$\Delta\boldsymbol{\Lambda}^{l_{k\cdot j}} = \boldsymbol{\Lambda}^{l_{k\cdot j}}_{t_{i+1}} - \boldsymbol{\Lambda}^{l_{k\cdot j}}_{t_i} \qquad \forall t_i \in \{1, m_k\} \quad \Delta\boldsymbol{\Lambda}^{l_{j\cdot k}} = \boldsymbol{\Lambda}^{l_{j\cdot k}}_{t_{j+1}} - \boldsymbol{\Lambda}^{l_{j\cdot k}}_{t_j} \qquad \forall t_j \in \{1, m_j\} \tag{16a, b}$$

where $\Delta\boldsymbol{\Lambda}^{l_{k\cdot j}}$ and $\Delta\boldsymbol{\Lambda}^{l_{j\cdot k}}$ refer to the link force increments of the kth and jth subdomains, respectively. The total link forces over the system time step ΔT have the following relationship.

$$\Delta\boldsymbol{\Lambda}^{K\cdot J} = m_k \quad \Delta\boldsymbol{\Lambda}^{l_{k\cdot j}} = m_j\Delta\boldsymbol{\Lambda}^{l_{j\cdot k}} \tag{17}$$

So far, the coupling dynamic system is built at different temporal (i.e., Equation (9)) and element scales (i.e., Equation 14).[34] The number of link forces (i.e., unknown quantities) is identical to the number of the velocity continuity conditions. Responses and link forces of the coupling system are only calculated at the system time step (i.e., t_n and t_{n+1}), as shown in Figure 2. If interface link forces are obtained, subdomains can be decomposed into independent subdomains with different time steps (see Figure 1B), and independent substructures with various integration parameters can be combined into an entire calculational domain (see Figure 1C). Therefore, to decouple the coupling system or couple independent computational substructures, the following method is formulated to solve the interface link forces at the system time step.

3 | PROPOSITION OF THE PARTITIONED/COMBINED COMPUTATIONAL METHOD

Link forces between the interconnected subdomains are calculated in this section. Specifically, firstly, velocity increments within ΔT are computed based on the initial information at t_n. Interface link forces are then obtained using the velocity continuity conditions.

3.1 | Velocity increment within the system time step

The jth subdomain with m_j time sub-steps (see Figure 2) is used to illustrate the calculation of velocity increments within ΔT. The incremental form of the interface-based dynamic equation without damping is written as:

$$\boldsymbol{M}\Delta\boldsymbol{a}_{t_{j+1}} + \boldsymbol{K}\Delta\boldsymbol{u}_{t_{j+1}} + \mathbb{L}^T\Delta\mathfrak{R}_{t_{j+1}} = \Delta\boldsymbol{P}_{t_{j+1}} \tag{18}$$

where $\Delta\mathfrak{R}_{t_{j+1}}$ refers to the link forces applied to the jth subdomain at the time sub-step t_{j+1}, which are given in Equation (14b). It is worth noting that only the jth subdomain is involved in the calculation process of velocity increments, and the superscript j of all quantities is thus ignored temporarily in the derivation process of the link force. Moreover, the link force increment at each time sub-step for the given interface is assumed to be constant (see Equation (17)), therefore, the subscript of the link force is simplified as $\Delta\mathfrak{R}$. Substituting incremental Newmark scheme (Equation 11) into Equation (18), velocity increments are obtained as follows:

$$\Delta\boldsymbol{v}_{t_{j+1}} = \boldsymbol{K}^{*^{-1}}\left(\Delta\boldsymbol{P}_{t_{j+1}} - \mathbb{L}^T\Delta\mathfrak{R} - \boldsymbol{R}^*\boldsymbol{a}_{t_j} - \Delta h\boldsymbol{K}\boldsymbol{v}_{t_j}\right) \tag{19a}$$

$$\boldsymbol{K}^* = \frac{1}{\gamma\Delta h}\boldsymbol{M} + \frac{\beta\Delta h}{\gamma}\boldsymbol{K} \quad \boldsymbol{R}^* = \frac{\gamma-2\beta}{2\gamma}\Delta h^2\boldsymbol{K} - \frac{1}{\gamma}\boldsymbol{M} \tag{19b}$$

To solve velocity responses using the initial information, replacing velocity (i.e., $\boldsymbol{v}t_j$) and acceleration (i.e., $\boldsymbol{a}t_j$) elements at the right side of Equation (19a) by $\Delta\boldsymbol{v}t_j + \boldsymbol{v}t_{j\text{-}1}$ and $\Delta\boldsymbol{a}t_j + \boldsymbol{a}t_{j\text{-}1}$, respectively, a recursive expression of the velocity increment is obtained as follows:

$$\Delta\boldsymbol{v}_{t_{j+1}} = \boldsymbol{K}^{*^{-1}}\left(\Delta\boldsymbol{P}_{t_{j+1}} - \Delta\boldsymbol{P}_{t_j} - \boldsymbol{R}^*\Delta\boldsymbol{a}_{t_j} - \left(\Delta h\boldsymbol{K} - \boldsymbol{K}^*\right)\Delta\boldsymbol{v}_{t_j}\right) \qquad \left(t_j = \{1, 2 \ \ldots \ m_j\}\right) \tag{20}$$

To remove the increment of accelerations at Equation (20), Equation (11b) is rewritten as follows:

$$\Delta\boldsymbol{a}_{t_{j+1}} = \frac{1}{\gamma\Delta h}\Delta\boldsymbol{v}_{t_{j+1}} - \frac{1}{\gamma}\left(\Delta\boldsymbol{a}_{t_j} + \boldsymbol{a}_{t_{j-1}}\right) \tag{21}$$

The acceleration increment $\Delta\boldsymbol{a}t_{j\text{-}1}$ within ΔT is calculated as:

$$\Delta\boldsymbol{a}_{t_{j+1}} = \frac{1}{\gamma\Delta h}\left(\Delta\boldsymbol{v}_{t_{j+1}} - \frac{1}{\gamma}\sum_{i=1}^{j}\left(\frac{\gamma-1}{\gamma}\right)^{i-1}\Delta\boldsymbol{v}_{t_{j+1-i}}\right) - \frac{1}{\gamma}\left(\frac{\gamma-1}{\gamma}\right)^{j}\boldsymbol{a}_0 \qquad \left(t_j = \{0, 1 \ \ldots \ m_j\}\right) \tag{22}$$

Substituting Equation (22) into Equation (20), the velocity increment is written as follows:

$$\Delta\boldsymbol{v}_{t_{j+1}} = \boldsymbol{K}^{*^{-1}}\left(\Delta\boldsymbol{P}_{t_{j+1}} - \Delta\boldsymbol{P}_n + \frac{1}{\gamma}\left(\frac{\gamma-1}{\gamma}\right)^{j-1}\boldsymbol{R}^*\boldsymbol{a}_0 + \frac{\boldsymbol{R}^*}{\Delta h\gamma^2}\sum_{i=1}^{j-1}\left(\frac{\gamma-1}{\gamma}\right)^{i-1}\Delta\boldsymbol{v}_{t_{j-i}} - \boldsymbol{G}\Delta\boldsymbol{v}_{t_j}\right) \tag{23a}$$

$$\boldsymbol{G} = \Delta h\left(\beta\frac{1+\gamma}{\gamma^2} - \frac{1+2\gamma}{2\gamma}\right)\boldsymbol{K} + \frac{1+\gamma}{\Delta h\gamma^2}\boldsymbol{M} \tag{23b}$$

Substituting the velocity solved at the previous steps into Equation (23) and simplifying them, the velocity increment at arbitrary time step t_{n+1} is calculated as follows:

$$\Delta \boldsymbol{v}_{t_{n+1}} = \sum_{i=1}^{n} \boldsymbol{A}_{t_i} \left(\Delta \boldsymbol{P}_{t_{n+2-i}} - \Delta \boldsymbol{P}_{t_{n+1-i}} + \frac{1}{\gamma} \left(\frac{\gamma - 1}{\gamma} \right)^{n-i} \boldsymbol{R}^* \boldsymbol{a}_{t_0} \right) + \boldsymbol{A}_{t_{n+1}} \boldsymbol{K}^* \Delta \boldsymbol{v}_{t_1} \tag{24a}$$

$$\boldsymbol{A}_{t_{i+1}} = \boldsymbol{A}_{t_1} \left(\boldsymbol{G}\ \boldsymbol{A}_{t_i} + \frac{1}{\Delta h \gamma^2} \boldsymbol{R}^* \sum_{f=1}^{i-1} \left(\frac{\gamma - 1}{\gamma} \right)^{i-1-k} \boldsymbol{A}_{t_f} \right) \quad \left(t_i = \{1 \ \dots \ m_j - 1\} \right) \quad \boldsymbol{A}_{t_1} = \boldsymbol{K}^{*^{-1}}. \tag{24b}$$

By adding up all velocity increments over ΔT, the total velocity increment $\Delta \boldsymbol{V}$ is solved as:

$$\Delta \boldsymbol{V} = \sum_{t_{ii}=1}^{m_j - 1} \left(\left(\sum_{t_i=1}^{ii} \boldsymbol{A}_{t_i} \right) \left(\Delta \boldsymbol{P}_{m_j+1-t_{ii}} - \Delta \boldsymbol{P}_{m_j - t_{ii}} + \frac{1}{\gamma} \left(\frac{\gamma - 1}{\gamma} \right)^{m_j - 1 - t_{ii}} \boldsymbol{R}^* \boldsymbol{a}_{t_0} \right) \right) + \left(\sum_{t_i=1}^{m_j} \boldsymbol{A}_{t_i} \right) \boldsymbol{K}^* \Delta \boldsymbol{v}_{t_1} \tag{25}$$

Simplifying coefficients at Equation (25), the total velocity increment is rewritten as:

$$\Delta \boldsymbol{V} = \sum_{t_{ii}=1}^{m_j - 1} \boldsymbol{b}_{m_j+1-t_{ii}} \boldsymbol{F}_{t_{ii}} + \boldsymbol{b}_{t_1} \boldsymbol{K}^* \Delta \boldsymbol{v}_{t_1} \tag{26a}$$

$$\boldsymbol{b}_i = \sum_{t_f=1}^{m_j+1-i} \boldsymbol{A}_{t_f} \qquad t_i = \{1, , , m_j\}\ , \ \boldsymbol{F}_{t_{ii}} = \left(\Delta \boldsymbol{P}_{m_j+1-t_{ii}} - \Delta \boldsymbol{P}_{m_j - t_{ii}} + \frac{1}{\gamma} \left(\frac{\gamma - 1}{\gamma} \right)^{m_j - 1 - t_{ii}} \boldsymbol{R}^* \boldsymbol{a}_{t_0} \right) \tag{26b}$$

As shown in Equation (26), the velocity increment of the system time step is solved by using the initial information at t_n (i.e., $\Delta \boldsymbol{v} t_1$ and $\boldsymbol{a} t_0$). To solve the link forces in the next subsection, the first velocity increment $\Delta \boldsymbol{v} t_1$ is divided into two parts, that is, $\Delta \bar{\boldsymbol{v}} t_1$ and $\Delta \boldsymbol{w} t_1$, as follows:

$$\Delta \boldsymbol{v}_{t_1} = \Delta \bar{\boldsymbol{v}}_{t_1} + \Delta \boldsymbol{w}_{t_1} \tag{27a}$$

$$\Delta \bar{\boldsymbol{v}}_{t_1} = \boldsymbol{K}^{*^{-1}} \left(\Delta \boldsymbol{P}_{t_1} - \boldsymbol{R}^* \boldsymbol{a}_{t_0} - \Delta h \boldsymbol{K} \boldsymbol{v}_{t_0} \right) \quad \Delta \boldsymbol{w}_{t_1} = -\boldsymbol{K}^{*^{-1}} \boldsymbol{L}^T \Delta \mathfrak{R} \tag{27b}$$

Substituting Equation (27) into Equation (26), the total velocity increment at ΔT is divided into two parts, that is, $\Delta \overline{\boldsymbol{V}}$ and $\Delta \boldsymbol{W}$, which can be, respectively, written as follows:

$$\Delta \boldsymbol{V} = \Delta \overline{\boldsymbol{V}} + \Delta \boldsymbol{W} \tag{28a}$$

$$\Delta \overline{\boldsymbol{V}} = \sum_{t_{ii}=1}^{m_j - 1} \boldsymbol{b}_{m_j+1-t_{ii}} \boldsymbol{F}_{t_{ii}} + \boldsymbol{b}_{t_1} \boldsymbol{K}^* \Delta \bar{\boldsymbol{v}}_{t_1} \quad \Delta \boldsymbol{W} = -\boldsymbol{b}_{t_1} \boldsymbol{L}^T \Delta \mathfrak{R} \tag{28b}$$

Except for external excitations $\boldsymbol{F} t_{ii}$, other coefficients at Equation (28) are constant for a linear system, which can be given before operations.

3.2 | Calculation of the interface link force

The lth interface, interconnecting with the kth and the jth subdomains (see Fig. b), is employed to illustrate the calculation process of interface link forces by using the velocity continuity conditions (Equation (15)) and velocity increments solved (Equation 28). The velocity continuity condition at the lth interface is rewritten as:

$$\sum_{t_i=1}^{m_k} \boldsymbol{L}_l^{k \cdot j} \Delta \boldsymbol{v}_{t_i}^k + \sum_{t_i=1}^{m_j} \boldsymbol{L}_l^{j \cdot k} \Delta \boldsymbol{v}_{t_i}^j = 0 \tag{29}$$

Velocity increments at time sub-steps are divided into free vibrations and link vibrations to calculate interface link forces, and Equation (29) is rewritten as:

$$\sum_{t_i=1}^{m_k} \boldsymbol{L}_l^{k\cdot j}\left(\Delta\overline{\boldsymbol{v}}_{t_i}^k + \Delta\boldsymbol{w}_{t_i}^k\right) + \sum_{t_i=1}^{m_j} \boldsymbol{L}_l^{j\cdot k}\left(\Delta\overline{\boldsymbol{v}}_{t_i}^j + \Delta\boldsymbol{w}_{t_i}^j\right) = 0 \tag{30}$$

Using Equation (28), the velocity increments under link forces are solved as follows:

$$\Delta\boldsymbol{w}_{t_i}^k = -\boldsymbol{b}_{t_1}^k \boldsymbol{L}_l^{k\cdot j^T} \Delta\mathfrak{R}^k \quad \Delta\boldsymbol{w}_{t_i}^j = -\boldsymbol{b}_{t_1}^j \boldsymbol{L}_l^{j\cdot k^T} \Delta\mathfrak{R}^j. \tag{31a, b}$$

Substituting the link forces in Equation (9) into Equation (31), one has:

$$\Delta\boldsymbol{w}_{t_i}^k = -\boldsymbol{b}_{t_1}^k \sum_{l=1}^{S_k} \boldsymbol{L}_l^{k\cdot j^T} \Delta\boldsymbol{\Lambda}^{l_{k\cdot j}} \quad \Delta\boldsymbol{w}_{t_i}^j = -\boldsymbol{b}_{t_1}^j \sum_{l=1}^{S_j} \boldsymbol{L}_l^{j\cdot k^T} \Delta\boldsymbol{\Lambda}^{l_{j\cdot k}}. \tag{32a, b}$$

As shown in Equation (32a), the kth subdomain is interconnected with S_k subdomains. The link forces of the kth subdomains are divided into two parts, as presented in Equation (32a). Similar treatments are performed for the jth subdomain. Therefore, Equation (32) is rewritten as follows:

$$\Delta\boldsymbol{w}_{t_i}^k = -\boldsymbol{b}_{t_1}^k \boldsymbol{L}_l^{k\cdot j^T} \boldsymbol{\Lambda}^{l_{k\cdot j}} - \boldsymbol{b}_{t_1}^k \sum_{l=1\ (f\neq j)}^{S_k-1} \boldsymbol{L}_l^{k\cdot f^T} \boldsymbol{\Lambda}^{l_{k\cdot f}} \quad \Delta\boldsymbol{w}_{t_i}^j = -\boldsymbol{b}_{t_1}^j \boldsymbol{L}_l^{j\cdot k^T} \boldsymbol{\Lambda}^{l_{j\cdot k}} - \boldsymbol{b}_{t_1}^j \sum_{l=1\ (f\neq k)}^{S_j-1} \boldsymbol{L}_l^{j\cdot f^T} \boldsymbol{\Lambda}^{l_{j\cdot f}}. \tag{33a, b}$$

Using Equation (28b), the velocity increments under external excitations are solved as:

$$\Delta\overline{\boldsymbol{V}}^k = \boldsymbol{b}_{t_1}^k \boldsymbol{K}^{*k} \Delta\overline{\boldsymbol{v}}_{t_1}^k + \sum_{t_{ii}=1}^{m_k-1} \boldsymbol{b}_{m_k+1-t_{ii}} \boldsymbol{F}_{t_{ii}}^k \quad \Delta\overline{\boldsymbol{V}}^j = \boldsymbol{b}_{t_1}^j \boldsymbol{K}^{*j} \Delta\overline{\boldsymbol{v}}_{t_1}^j + \sum_{t_{ii}=1}^{m_j-1} \boldsymbol{b}_{m_j+1-t_{ii}} \boldsymbol{F}_{t_{ii}}^j. \tag{34a, b}$$

Substituting Equations (16), (33), and (34) into the velocity continuity condition built at the system time step t_{n+1} (i.e., Equation (29)), one has:

$$\sum_{t_i=1}^{m_k} \boldsymbol{L}_l^{k\cdot j} \Delta\overline{\boldsymbol{v}}_{t_i}^k + \sum_{t_i=1}^{m_j} \boldsymbol{L}_l^{j\cdot k} \Delta\overline{\boldsymbol{v}}_{t_i}^j = \left(\frac{1}{m_k}\sum_{t_i=1}^{m_k} \boldsymbol{L}_l^{k\cdot j} \boldsymbol{b}_{t_1}^k \boldsymbol{L}_l^{k\cdot j^T} + \frac{1}{m_j}\sum_{t_i=1}^{m_j} \boldsymbol{L}_l^{j\cdot k} \boldsymbol{b}_{t_1}^j \boldsymbol{L}_l^{j\cdot k^T}\right) \Delta\boldsymbol{\Lambda}_{t_{n+1}}^{K\cdot J_l} + \partial\boldsymbol{v}_{K\cdot J} \tag{35a}$$

$$\partial\boldsymbol{v}_{K\cdot J} = \sum_{l=1\ (f\neq j)}^{S_k-1} \left(\frac{1}{m_k}\sum_{t_i=1}^{m_k} \boldsymbol{L}_l^{k\cdot j} \boldsymbol{b}_{t_1}^k \boldsymbol{L}_l^{k\cdot f^T}\right) \Delta\boldsymbol{\Lambda}_{t_{n+1}}^{K\cdot f_l} + \sum_{l=1\ (f\neq k)}^{S_j-1} \left(\frac{1}{m_j}\sum_{t_i=1}^{m_j} \boldsymbol{L}_l^{j\cdot k} \boldsymbol{b}_{t_1}^j \boldsymbol{L}_l^{j\cdot f^T}\right) \Delta\boldsymbol{\Lambda}_{t_{n+1}}^{J\cdot f_l} \tag{35b}$$

where $\partial\boldsymbol{v}$ refers to the additional velocity increment. All link force increments at time sub-steps are transferred into link force increments at the system time step ΔT. By substituting Equations (34) and (37) into Equation (29), one gets:

$$\overline{\boldsymbol{V}}_{K\cdot J} = \boldsymbol{H}_{K\cdot J} \Delta\boldsymbol{\Lambda}^{K\cdot J} + \sum_{l=1\ (f\neq j)}^{S_k-1} \boldsymbol{H}_{K\cdot f_l} \Delta\boldsymbol{\Lambda}^{K\cdot f_l} + \sum_{l=1\ (f\neq k)}^{S_j-1} \boldsymbol{H}_{J\cdot f_l} \Delta\boldsymbol{\Lambda}^{J\cdot f_l} \tag{36}$$

where the coefficients are:

$$\overline{\boldsymbol{V}}_{K\cdot J} = \boldsymbol{L}_l^{k\cdot j} \Delta\overline{\boldsymbol{V}}^k + \boldsymbol{L}_l^{j\cdot k} \Delta\overline{\boldsymbol{V}}^j \quad \boldsymbol{H}_{K\cdot J} = \left(\frac{1}{m_k}\sum_{t_i=1}^{m_k} \boldsymbol{L}_l^{k\cdot j} \boldsymbol{b}_{t_1}^k \boldsymbol{L}_l^{k\cdot j^T} + \frac{1}{m_j}\sum_{t_j=1}^{m_j} \boldsymbol{L}_l^{j\cdot k} \boldsymbol{b}_{t_1}^j \boldsymbol{L}_l^{j\cdot k^T}\right) \tag{37a}$$

$$\boldsymbol{H}_{K\cdot f_l} = \frac{1}{m_k}\sum_{t_i=1}^{m_k} \boldsymbol{L}_l^{k\cdot j} \boldsymbol{b}_{t_1}^k \boldsymbol{L}_l^{k\cdot f^T} \quad \boldsymbol{H}_{J\cdot f_l} = \frac{1}{m_j}\sum_{t_i=1}^{m_j} \boldsymbol{L}_l^{j\cdot k} \boldsymbol{b}_{t_1}^j \boldsymbol{L}_l^{j\cdot f^T} \tag{37b}$$

It is worth noting that for a linear system, except for $\overline{\boldsymbol{V}}_{K\cdot J}$ at Equation (37a), other coefficients are constant, which can be given before a calculation. Furthermore, for the system with only two subdomains/substructures, the velocity continuity condition is written as follows:

$$\boldsymbol{L}_l^{k\cdot j}\Delta\overline{\boldsymbol{V}}^k+\boldsymbol{L}_l^{j\cdot k}\Delta\overline{\boldsymbol{V}}^j=\left(\frac{1}{m_k}\sum_{t_i=1}^{m_k}\boldsymbol{L}_l^{k\cdot j}\boldsymbol{b}_{t_1}^k\boldsymbol{L}_l^{k\cdot j^T}+\frac{1}{m_j}\sum_{t_j=1}^{m_j}\boldsymbol{L}_l^{j\cdot k}\boldsymbol{b}_{t_1}^j\boldsymbol{L}_l^{j\cdot k^T}\right)\Delta\boldsymbol{\Lambda}_{t_{n+1}}^{K\cdot J_l} \tag{38}$$

Equation (38) is simplified as:

$$\boldsymbol{H}_{K\cdot J}\Delta\boldsymbol{\Lambda}^{K\cdot J}=\overline{\boldsymbol{V}}_{K\cdot J} \tag{39}$$

where the coefficients are designed as follows:

$$\overline{\boldsymbol{V}}_{K\cdot J}=\boldsymbol{L}_l^{k\cdot j}\Delta\overline{\boldsymbol{V}}^k+\boldsymbol{L}_l^{j\cdot k}\Delta\overline{\boldsymbol{V}}^j\ \boldsymbol{H}_{K\cdot J}=\left(\frac{1}{m_k}\sum_{t_i=1}^{m_k}\boldsymbol{L}_l^{k\cdot j}\boldsymbol{b}_{t_1}^k\boldsymbol{L}_l^{k\cdot j^T}+\frac{1}{m_j}\sum_{t_j=1}^{m_j}\boldsymbol{L}_l^{j\cdot k}\boldsymbol{b}_{t_1}^j\boldsymbol{L}_l^{j\cdot k^T}\right) \tag{40}$$

So far, the link forces at the lth interface are solved. For a domain with S subdomains, $\tilde{S}$ velocity continuity conditions (Equation 15) are imposed on corresponding interfaces. Therefore, $\tilde{S}$ link forces can be written into linear equations as follows:

$$\boldsymbol{L}_l^{k\cdot j}\Delta\overline{\boldsymbol{V}}^k+\boldsymbol{L}_l^{j\cdot k}\Delta\overline{\boldsymbol{V}}^j=\boldsymbol{H}_{K\cdot J}\Delta\boldsymbol{\Lambda}_{t_{n+1}}^{K\cdot J_l}+\partial\boldsymbol{v}_{K\cdot J}\qquad\forall\quad l\in\{1,,,\tilde{S}\} \tag{41}$$

All interface link forces are solved by using Equation (41). By using the solved link forces, the coupling system can be decomposed into several independent computational subdomains (i.e., partitioned calculation, see Figure 1A,B), and each independent substructure can be combined into an entire computational domain (i.e., combined calculation, see Figure 1B,C).

3.3 | Implementation of the proposed method

Interface link forces are calculated by using Equation (41). Therefore, each subdomain at time sub-steps can be solved independently and be coupled at the system time step, and freely combined computations of different substructures can be conducted. Independent dynamic equations are written as follows:

$$\begin{cases}\mathbb{K}_*^1\Delta\mathbb{U}_{t_i}^1=\mathbb{F}_{t_i}^1-\mathbb{L}_1^T\Delta\mathfrak{R}_{t_i}^1 & \forall t_i\in\{1,m_i\}\\ \vdots & \\ \mathbb{K}_*^k\Delta\mathbb{U}_{t_k}^k=\mathbb{F}_{t_k}^k-\mathbb{L}_k^T\Delta\mathfrak{R}_{t_k}^k & \forall t_k\in\{1,m_k\}\\ \vdots & \\ \mathbb{K}_*^S\Delta\mathbb{U}_{t_S}^S=\mathbb{F}_{t_S}^S-\mathbb{L}_{t_S}^T\Delta\mathfrak{R}_{t_S}^S & \forall t_S\in\{1,m_S\}\end{cases} \tag{42}$$

To detail the implementation process of the new proposed method, the detailed calculation procedure is given in Table A1.

4 | ENERGY INVESTIGATION OF THE PROPOSED METHOD

4.1 | Discussion of the interface pseudo-energy

The following pseudo-energy norm[32] is employed to demonstrate the stability of the proposed method with Newmark scheme:

$$\left[\frac{1}{2}\boldsymbol{a}^{k^T}\overline{\boldsymbol{A}}^k\boldsymbol{a}^k+\frac{1}{2}\boldsymbol{v}^{k^T}\boldsymbol{K}^k\boldsymbol{v}^k\right]_{t_n}^{t_{n+1}}=-\left(\gamma^k-\frac{1}{2}\right)\Delta\boldsymbol{a}_{t_{n+1}}^{k^T}\overline{\boldsymbol{A}}^k\Delta\boldsymbol{a}_{t_{n+1}}^k+\frac{1}{\Delta h^k}\Delta\boldsymbol{v}_{t_{n+1}}^{k^T}\Delta\boldsymbol{R}_{t_{n+1}}^k \tag{43}$$

$$\overline{\boldsymbol{A}}^k = \boldsymbol{M}^k + \Delta h^{k^2}\left(\beta^k - \frac{1}{2}\gamma^k\right)\boldsymbol{K}^k \quad \Delta \boldsymbol{R}^k = \Delta \boldsymbol{P}^k_{t_{n+1}} + \sum_{l=1}^{S_k} \boldsymbol{L}_l^{k\cdot j^T} \boldsymbol{\Lambda}^{l_{k\cdot j}}_{t_{n+1}} \tag{44}$$

where the symbol [ ] is the increment of kinematic quantities from time step t_n to t_{n+1}. Note that damping is ignored in the expression, and link forces $\sum_{l=1}^{S_k} \boldsymbol{\Lambda}^{l_{k\cdot j}}_{t_{n+1}}$ and external excitations $\Delta \boldsymbol{P}^k_{t_{n+1}}$ are acted on the kth subdomain. Further details on the pseudo-energy can be found in Reference 3. The incremental form of Equation (44) is:

$$\Delta E^k_{kin} + \Delta E^k_{\text{int}} = \Delta E^k_{diss} + \Delta E^k_{ext} \tag{45a}$$

$$\Delta E^k_{kin} = \left[\frac{1}{2}\boldsymbol{a}^{k^T}\overline{\boldsymbol{A}}^k\boldsymbol{a}^k\right]_{t_n}^{t_{n+1}} \quad \Delta E^k_{int} = \left[\frac{1}{2}\boldsymbol{v}^{k^T}\boldsymbol{K}^k\boldsymbol{v}^k\right]_{t_n}^{t_{n+1}} \tag{45b}$$

$$\Delta E^k_{diss} = -\left(\gamma^k - \frac{1}{2}\right)\Delta \boldsymbol{a}^{k^T}_{t_{n+1}}\overline{\boldsymbol{A}}^k\Delta \boldsymbol{a}^k_{t_{n+1}} \quad \Delta E^k_{ext} = \frac{1}{\Delta h^k}\Delta \boldsymbol{v}^{k^T}_{t_{n+1}}\boldsymbol{L}_l^{k\cdot j^T}\Delta \boldsymbol{R}^k_{t_{n+1}} \tag{45c}$$

The system without external excitations is used to discuss the stability of the proposed method. For the kth subdomain, the pseudo-energy ΔE^k_{ext} generated by link forces is:

$$\Delta E^k_{link} = \Delta E^k_{ext} = \frac{1}{\Delta h^k}\Delta \boldsymbol{v}^{k^T}_{t_{n+1}}\boldsymbol{L}_l^{k\cdot j^T}\sum_{l=1}^{S_k}\Delta \boldsymbol{\Lambda}^{l_{k\cdot j}}_{t_{n+1}} \tag{46}$$

According to the requirements of stability derived in Reference 3 (i.e., $\gamma \geq 1/2$ and $\overline{\boldsymbol{A}}$ is positive definite), the stability of an individual subdomain under link forces can be ensured if $\Delta E^k_{ext} \leq 0$. Therefore, to ensure the stability of the kth subdomain, $\Delta E^k_{link} \leq 0$ (i.e., Equation 46) is required. Referring to Equation (45), for the entire system with S subdomains and different time sub-steps, the total pseudo-energy within the system time step can be derived as follows:

$$\sum_{k=1}^{S}\left(\sum_{t_k=1}^{m_k}\left(\Delta E^k_{kin,t_k} + \Delta E^k_{int,t_k}\right)\right) = \sum_{k=1}^{S}\left(\sum_{t_k=1}^{m_k}\left(\Delta E^k_{diss,t_k}\right)\right) + \Delta E_{link} \tag{47}$$

The total pseudo-energy dissipated at all interfaces is calculated as follows:

$$\Delta E_{link} = \sum_{l=1}^{\tilde{S}}\left(\sum_{t_k=1}^{m_k}\left(\Delta E^{k\cdot j}_{ext,t_k}\right) + \sum_{t_j=1}^{m_j}\left(\Delta E^{j\cdot k}_{ext,t_j}\right)\right) \tag{48}$$

Substituting Equation (46) into Equation (48), the total pseudo-energy dissipated at all interfaces is:

$$\Delta E_{link} = \sum_{l=1}^{\tilde{S}}\left(\sum_{t_k=1}^{m_k}\frac{1}{\Delta h^k}\Delta \boldsymbol{v}^{k^T}_{t_k}\boldsymbol{L}_l^{k\cdot j^T}\left(\boldsymbol{\Lambda}^{l_{k\cdot j}}_{t_k} - \boldsymbol{\Lambda}^{l_{k\cdot j}}_{t_{k-1}}\right) + \sum_{t_j=1}^{m_j}\frac{1}{\Delta h^j}\Delta \boldsymbol{v}^{j^T}_{i\cdot j}\boldsymbol{L}_l^{j\cdot k^T}\left(\boldsymbol{\Lambda}^{l_{j\cdot k}}_{t_j} - \boldsymbol{\Lambda}^{l_{j\cdot k}}_{t_{j-1}}\right)\right) \tag{49}$$

Using the assumption of link forces (i.e., Equation 16) and the time step ratios, the total pseudo-energy is simplified as follows:

$$\Delta E_{link} = \frac{1}{\Delta T}\sum_{l=1}^{\tilde{S}}\left(\left(\sum_{t_k=1}^{m_k}\Delta \boldsymbol{v}^{k^T}_{t_k}\boldsymbol{L}_l^{k\cdot j^T} + \sum_{t_j=1}^{m_j}\Delta \boldsymbol{v}^{j^T}_{t_j}\boldsymbol{L}_l^{j\cdot k^T}\right)\Delta \boldsymbol{\Lambda}^{K\cdot J_l}\right) \tag{50}$$

Substituting velocity continuity conditions Equation (29) into Equation (50), one has:

$$\Delta E_{link} = 0 \tag{51}$$

Therefore, when the linear interpolation assumption of link forces (i.e., Equation 16) and the velocity continuity conditions (i.e., Equation 29) are fulfilled at all interfaces, the total interface pseudo-energy generated by link forces is equal to zero; algorithmic parameters do not influence the interface pseudo-energy; and the system stability can be ensured. It is worth noting that due to floating-point operation errors, tiny pseudo-energy is generated and accumulated along with time, which would be further studied in the numerical demonstration.

4.2 | Investigation of the interface mechanical energy

The following classical mechanical energy generated by link forces and algorithmic parameters is used to further investigate the interface energy of the dynamic system calculated by the proposed method with Newmark scheme. Further information can be found in Reference 32.

$$\left[\frac{1}{2}\boldsymbol{v}^T\boldsymbol{M}\boldsymbol{v}+\frac{1}{2}\boldsymbol{u}^T\boldsymbol{K}\boldsymbol{u}\right]_{t_n}^{t_{n+1}}=\Delta\boldsymbol{u}^T\left(\gamma\boldsymbol{P}_{t_{n+1}}+(1-\gamma)\boldsymbol{P}_{t_n}\right)-\left(\gamma-\frac{1}{2}\right)\Delta\boldsymbol{u}^T\boldsymbol{K}\Delta\boldsymbol{u}$$
$$-\left(\gamma-\frac{1}{2}\right)\left(\beta-\frac{1}{2}\gamma\right)\Delta h^2\Delta\boldsymbol{a}^T\boldsymbol{M}\Delta\boldsymbol{a}-\left(\beta-\frac{1}{2}\gamma\right)\frac{1}{2}\Delta h^2\left[\boldsymbol{a}^T\boldsymbol{M}\boldsymbol{a}\right]_{t_n}^{t_{n+1}} \tag{52}$$

The mechanical energy increment of the kth subdomain is written as follows:

$$\Delta\tau_{t_i}^k+\Delta v_{t_i}^k=\Delta\boldsymbol{u}_{t_i}^{k^T}\sum_{l=1}^{S_k}\boldsymbol{L}_l^{k\cdot j^T}\left(\gamma^k\boldsymbol{\Lambda}_{t_{i+1}}^{l_{k\cdot j}}+\left(1-\gamma^k\right)\boldsymbol{\Lambda}_{t_i}^{l_{k\cdot j}}\right)-\left(\gamma^k-\frac{1}{2}\right)\Delta\boldsymbol{u}_{t_i}^{k^T}\boldsymbol{K}\Delta\boldsymbol{u}_{t_i}^k$$
$$-\left(\gamma^k-\frac{1}{2}\right)\left(\beta^k-\frac{1}{2}\gamma^k\right)\Delta h^{k^2}\Delta\boldsymbol{a}_{t_i}^{k^T}\boldsymbol{M}\Delta\boldsymbol{a}_{t_i}^k-\left(\beta^k-\frac{1}{2}\gamma^k\right)\Delta o_{t_i}^k \tag{53a}$$

$$\Delta\tau_i^k=\frac{1}{2}\boldsymbol{v}_{t_{i+1}}^{k^T}\boldsymbol{M}\boldsymbol{v}_{t_{i+1}}^k-\frac{1}{2}\boldsymbol{v}_{t_i}^{k^T}\boldsymbol{M}\boldsymbol{v}_{t_i}^k\quad\Delta v_{t_i}^k=\frac{1}{2}\boldsymbol{u}_{t_{i+1}}^{k^T}\boldsymbol{K}\boldsymbol{u}_{t_{i+1}}^k-\frac{1}{2}\boldsymbol{u}_{t_i}^{k^T}\boldsymbol{K}\boldsymbol{u}_{t_i}^k \tag{53b}$$

$$\Delta o_{t_i}^k=\frac{1}{2}\Delta h^{k^2}\boldsymbol{a}_{t_{i+1}}^{k^T}\boldsymbol{M}\boldsymbol{a}_{t_{i+1}}^k-\frac{1}{2}\Delta h^{k^2}\boldsymbol{a}_{t_i}^{k^T}\boldsymbol{M}\boldsymbol{a}_{t_i}^k \tag{53c}$$

where $\Delta\tau_{t_i}^k$, $\Delta v_{t_i}^k$, and $\Delta o_{t_i}^k$ refer to the kinetic energy, the potential energy, and the dissipative energy increments for the kth subdomain at the t_i time step, respectively. External excitations are not considered in the analysis (i.e., $\boldsymbol{P}_n=\boldsymbol{P}_{n+1}=\boldsymbol{0}$). For the kth subdomain with m_k time steps and S_k interfaces, the mechanical energy increment over ΔT is calculated as:

$$\begin{aligned}\Delta Work^k&=\sum_{t_i=1}^{m_k}\left(\Delta\tau_{t_i}^k+\Delta v_{t_i}^k\right)\\&=\sum_{t_i=1}^{m_k}\Delta\boldsymbol{u}_{t_i}^{k^T}\sum_{l=1}^{S_k}\boldsymbol{L}_l^{k\cdot j^T}\left(\gamma^k\boldsymbol{\Lambda}_{t_{i+1}}^{l_{k\cdot j}}+\left(1-\gamma^k\right)\boldsymbol{\Lambda}_{t_i}^{l_{k\cdot j}}\right)-\left(\gamma^k-\frac{1}{2}\right)\sum_{t_i=1}^{m_k}\Delta\boldsymbol{u}_{t_i}^{k^T}\boldsymbol{K}\Delta\boldsymbol{u}_{t_i}^k\\&\quad-\left(\gamma^k-\frac{1}{2}\right)\left(\beta^k-\frac{1}{2}\gamma^k\right)\Delta h^{k^2}\sum_{t_i=1}^{m_k}\Delta\boldsymbol{a}_{t_i}^{k^T}\boldsymbol{M}\Delta\boldsymbol{a}_{t_i}^k-\left(\beta^k-\frac{1}{2}\gamma^k\right)\sum_{i=1}^{m_k}\Delta o_{t_i}^k\end{aligned} \tag{54}$$

The total increments of the system mechanical energy within ΔT for all subdomains are:

$$\Delta Work=\Delta W_{link}+\Delta W_{diss} \tag{55a}$$

$$\Delta W_{link}=\sum_{k=1}^{S}\sum_{t_i=1}^{m_k}\Delta\boldsymbol{u}_{t_i}^{k^T}\sum_{l=1}^{S_k}\boldsymbol{L}_l^{k\cdot j^T}\left(\boldsymbol{\Lambda}_{t_i}^{l_{k\cdot j}}+\gamma^k\Delta\boldsymbol{\Lambda}_{t_{i+1}}^{l_{k\cdot j}}\right) \tag{55b}$$

$$\begin{aligned}\Delta W_{diss}&=-\sum_{k=1}^{S}\left(\gamma^k-\frac{1}{2}\right)\sum_{t_i=1}^{m_k}\Delta\boldsymbol{u}_{t_i}^{k^T}\boldsymbol{K}\Delta\boldsymbol{u}_{t_i}^k\\&\quad-\sum_{k=1}^{S}\left(\gamma^k-\frac{1}{2}\right)\left(\beta^k-\frac{1}{2}\gamma^k\right)\Delta h^{k^2}\sum_{t_i=1}^{m_k}\Delta\boldsymbol{a}_{t_i}^{k^T}\boldsymbol{M}\Delta\boldsymbol{a}_{t_i}^k-\sum_{k=1}^{S}\left(\beta^k-\frac{1}{2}\gamma^k\right)\sum_{t_i=1}^{m_k}\Delta o_{t_i}^k\end{aligned} \tag{55c}$$

where ΔW_{link} and ΔW_{diss} are the interface mechanical energy generated by link forces and the algorithmic dissipation energy, respectively.[35] The algorithmic dissipation ΔW_{diss} is often used to filter high-frequency spurious vibration content.[36] Moreover, the mechanical energy increment ΔW_{link} of all interfaces is calculated as follows:

$$\Delta W_{link} = \sum_{l=1}^{\tilde{S}} \left(\sum_{t_k=1}^{m_k} \Delta \boldsymbol{u}_{t_k}^{k^T} \boldsymbol{L}_l^{k\cdot j^T} \left(\boldsymbol{\Lambda}_{t_k}^{l_{k\cdot j}} + \gamma^k \Delta \boldsymbol{\Lambda}_{t_{k+1}}^{l_{k\cdot j}} \right) + \sum_{t_j=1}^{m_j} \Delta \boldsymbol{u}_{t_j}^{j^T} \boldsymbol{L}_l^{j\cdot k^T} \left(\boldsymbol{\Lambda}_{t_j}^{l_{k\cdot j}} + \gamma^k \Delta \boldsymbol{\Lambda}_{t_{j+1}}^{l_{k\cdot j}} \right) \right) \tag{56}$$

The interface displacement elements (e.g., $\Delta \boldsymbol{u}_{t_k}^{k^T}$ and $\Delta \boldsymbol{u}_{t_j}^{j^T}$) are inconsistent, and thus the total interface mechanical energy may exist in interconnected interfaces. Furthermore, the second-order accuracy ($\gamma^k = 1/2$) is usually required in numerical results, hence, the system mechanical energy (Equation 55) can be rewritten as:

$$\Delta Work = \frac{1}{2} \sum_{l=1}^{\tilde{S}} \left(\begin{array}{l} \sum_{t_k=1}^{m_k} \Delta \boldsymbol{u}_{t_k}^{k^T} \boldsymbol{L}_l^{k\cdot j^T} \left(\boldsymbol{\Lambda}_{i_k}^{l_{k\cdot j}} + \boldsymbol{\Lambda}_{t_{k+1}}^{l_{k\cdot j}} \right) \\ + \sum_{t_j=1}^{m_j} \Delta \boldsymbol{u}_{t_j}^{j^T} \boldsymbol{L}_l^{j\cdot k^T} \left(\boldsymbol{\Lambda}_{t_j}^{l_{k\cdot j}} + \boldsymbol{\Lambda}_{t_{j+1}}^{l_{k\cdot j}} \right) \end{array} \right) - \sum_{k=1}^{S} \left(\beta^k - \frac{1}{4} \right) \sum_{t_k=1}^{m_k} \Delta o_{t_k}^k \tag{57}$$

Based on the expression of the system mechanical energy (i.e., Equation (57)), only when all subdomains have the constant time step ΔT and the same parameters $\beta^k = 1/4$, the system mechanical energy is conservative (i.e., $\Delta \text{work} = 0$).

5 | EXTENSION OF THE PROPOSED METHOD (GENERALIZED-α)

To obtain more desirable accuracy and algorithmic damping simultaneously, six integration schemes of Generalized-α (NG; i.e., NOCH-α, CH-α, NOHHT-α, HHT-α, NOWBZ-α, and WBZ-α) are investigated and incorporated into the proposed method above. More information on NG can be obtained in Reference 18. Specifically, link forces are firstly solved by using both the velocity increments and the velocity continuity conditions at the system time step. The coupling system is then decomposed into several independent subdomains using the solved link forces. The calculation of velocity increments and link forces, and the implementation of NG are successively discussed in this section.

5.1 | Calculation of the velocity increment

The incremental expressions of NG without damping[18] are:

$$\begin{aligned} &\boldsymbol{M}\left((1-\alpha)\Delta \boldsymbol{a}_{t_{n+1}} + \boldsymbol{a}_{t_n}\right) + \boldsymbol{K}\left((1-\eta)\Delta \boldsymbol{u}_{t_{n+1}} + \boldsymbol{u}_{t_n}\right) \\ &= (1-\eta)\Delta \boldsymbol{F}_{t_{n+1}} + \boldsymbol{F}_{t_n} - \boldsymbol{L}^T\left((1-\eta)\Delta \boldsymbol{\Lambda} + \boldsymbol{\Lambda}_{t_n}\right) \end{aligned} \tag{58a}$$

$$\Delta \boldsymbol{u}_{t_{n+1}} = \frac{\beta \Delta h}{\gamma} \Delta \boldsymbol{v}_{t_{n+1}} + \Delta h \boldsymbol{v}_{t_n} + \left(\varepsilon - \frac{\beta\mu}{\gamma}\right) \Delta h^2 \boldsymbol{a}_{t_n} \quad \Delta \boldsymbol{a}_{t_{n+1}} = \frac{1}{\Delta h \gamma} \Delta \boldsymbol{v}_{t_{n+1}} + \left(\frac{\mu}{\gamma} + 1\right) \boldsymbol{a}_{t_n} \tag{58b}$$

where α, δ, η, ε, β, μ, and γ are algorithmic parameters, which are used to adjust the accuracy and dissipation properties of NG. An individual subdomain with m sub-steps is investigated to calculate the velocity increment within the system time step. Note the superscript of all quantities is ignored due to the consideration of the individual subdomain. Using Equation (58), the velocity increment is derived as follows:

$$\overline{\boldsymbol{K}}^* \Delta \boldsymbol{v}_{t_{n+1}} = (1-\eta)\Delta \boldsymbol{F}_{t_{n+1}} + \boldsymbol{F}_{t_n} - \left(\boldsymbol{K}\boldsymbol{u}_{t_n} + (1-\eta)\Delta h \boldsymbol{K} \boldsymbol{v}_{t_n} + \overline{\boldsymbol{R}}^* \boldsymbol{a}_{t_n}\right) - \boldsymbol{L}^T\left((1-\eta)\Delta \boldsymbol{\Lambda} + \boldsymbol{\Lambda}_{t_n}\right) \tag{59a}$$

$$\overline{\boldsymbol{K}}^* = \left(\frac{(1-\alpha)}{\Delta h \gamma}\boldsymbol{M} + \frac{\Delta h \beta (1-\eta)}{\gamma}\boldsymbol{K}\right) \quad \overline{\boldsymbol{R}}^* = \left((1-\eta)\frac{(\gamma\varepsilon - \beta\mu)}{\gamma}\Delta h^2 \boldsymbol{K} + \frac{(\alpha(\gamma+\mu) - \mu)}{\gamma}\boldsymbol{M}\right) \tag{59b}$$

The first velocity increment is solved as follows:

$$\Delta \boldsymbol{v}_{t_1} = \overline{\boldsymbol{K}}^{*^{-1}} \left((1-\eta)\Delta \boldsymbol{F}_{t_1} + \boldsymbol{F}_{t_0} - \boldsymbol{L}^T \left((1-\eta)\Delta \boldsymbol{\Lambda} + \boldsymbol{\Lambda}_{t_0} \right) - \left(\boldsymbol{K}\boldsymbol{u}_{t_0} + (1-\eta)\Delta h \boldsymbol{K}\, \boldsymbol{v}_{t_0} + \overline{\boldsymbol{R}}^{*}\, \boldsymbol{a}_{t_0} \right) \right) \tag{60}$$

Using Equations (59a) and (59b), displacement and acceleration are, respectively, calculated as:

$$\Delta \boldsymbol{u}_{t_n} = \left(\left(\frac{-\mu}{\gamma} \right)^{n-1} \frac{\gamma\varepsilon - \beta\mu}{\gamma} \Delta h^2 \boldsymbol{a}_{t_0} + \Delta h \boldsymbol{v}_{t_0} + \sum_{i=1}^{n-1} \left(1 + \left(\frac{-\mu}{\gamma} \right)^{i-1} \frac{\gamma\varepsilon - \beta\mu}{\gamma^2} \right) \Delta h \Delta \boldsymbol{v}_{t_{n-i}} + \frac{\beta \Delta h}{\gamma} \Delta \boldsymbol{v}_{t_n} \right) \tag{61}$$

$$\Delta \boldsymbol{a}_{t_{n+1}} = \frac{1}{h\gamma} \left(\Delta \boldsymbol{v}_{t_n} - \frac{\gamma+\mu}{\gamma} \sum_{i=1}^{n-1} \left(\frac{-\mu}{\gamma} \right)^{i-1} \Delta \boldsymbol{v}_{t_{n-i}} \right) - \frac{\gamma+\mu}{\gamma} \left(\frac{-\mu}{\gamma} \right)^{n-1} \boldsymbol{a}_{t_0} \tag{62}$$

Substituting the solved displacement and acceleration into Equation (59), the velocity recursive function can be derived as:

$$\Delta \boldsymbol{v}_{t_{n+1}} = \overline{\boldsymbol{K}}^{*^{-1}} \begin{pmatrix} (1-\eta)\boldsymbol{F}_{t_{n+1}} + (2\eta-1)\boldsymbol{F}_{t_n} - \eta \boldsymbol{F}_{t_{n-1}} - \boldsymbol{L}^T \left((1-\eta)\Delta \boldsymbol{\Lambda} + \boldsymbol{\Lambda}_{t_n} \right) - \Delta h \boldsymbol{K} \boldsymbol{u}_{t_0} \\ - \left(\frac{-\mu}{\gamma} \right)^{n-1} \boldsymbol{\eta} \boldsymbol{a}_{t_0} + \boldsymbol{\mu} \Delta \boldsymbol{v}_{t_n} - \Delta h \sum_{i=1}^{n-1} \left(\boldsymbol{K} + \frac{1}{\gamma \Delta h^2} \left(\frac{-\mu}{\gamma} \right)^{i-1} \boldsymbol{\eta} \right) \Delta \boldsymbol{v}_{t_{n-i}} \end{pmatrix} \tag{63}$$

where coefficients matrices involved in Equation (62) are designed as:

$$\boldsymbol{\eta} = a_1 \boldsymbol{K} + a_2 \boldsymbol{M} \quad a_1 = \Delta h^2 \frac{(\gamma\varepsilon - \beta\mu)(\gamma\eta - (1-\eta)\mu)}{\gamma^2} \quad a_2 = \frac{(\gamma+\mu)(\mu - \alpha(\gamma+\mu))}{\gamma^2} \tag{64}$$

$$\boldsymbol{\mu} = a_3 \boldsymbol{M} + a_4 \boldsymbol{K} \quad a_3 = \frac{1-2\alpha}{\Delta h \gamma} + \frac{(1-\alpha)\mu}{\Delta h \gamma^2} \quad a_4 = \Delta h \left(\eta - 1 - \frac{\varepsilon(1-\eta) + \beta\eta}{\gamma} + \frac{\beta(1-\eta)\mu}{\gamma^2} \right) \tag{65}$$

Substituting the velocity increment solved at previous time-steps into Equation (63), the velocity increment at arbitrary time step t_{n+1} can be solved as follows:

$$\Delta \boldsymbol{v}_{t_{n+1}} = \sum_{i=1}^{n} \overline{\boldsymbol{A}}_i \begin{pmatrix} (1-\eta)\boldsymbol{F}_{t_{n+1}} + (2\eta-1)\boldsymbol{F}_{t_n} - \eta \boldsymbol{F}_{t_{n-1}} \\ - \boldsymbol{L}^T \Delta \boldsymbol{\Lambda} - \Delta h \boldsymbol{K} \boldsymbol{u}_{t_0} - \left(\frac{-\mu}{\gamma} \right)^{n-1} \boldsymbol{\eta}\, \boldsymbol{a}_{t_0} \end{pmatrix} + \overline{\boldsymbol{K}}^{*} \overline{\boldsymbol{A}}_{n+1} \boldsymbol{v}_{t_1} \tag{66a}$$

$$\overline{\boldsymbol{A}}_{i+1} = \overline{\boldsymbol{K}}^{*^{-1}} \left(\boldsymbol{\mu} \overline{\boldsymbol{A}}_i - \Delta h \sum_{i=1}^{n-1} \left(\boldsymbol{K} + \left(\frac{-\mu}{\gamma} \right)^{n-1-i} \frac{\boldsymbol{\eta}}{\gamma \Delta h^2} \right) \overline{\boldsymbol{A}}_i \right) \quad (i = \{1 \ \dots \ m-1\}) \ \ \overline{\boldsymbol{A}}_1 = \overline{\boldsymbol{K}}^{*^{-1}} \tag{66b}$$

By adding up all velocity increments and substituting $\Delta \boldsymbol{v} t_1$ into the sum, the total velocity increment within the system time step is solved as:

$$\Delta \boldsymbol{V} = \Delta \boldsymbol{V}_1 + \Delta \boldsymbol{V}_2 + \Delta \boldsymbol{V}_3 \tag{67a}$$

$$\Delta \boldsymbol{V}_1 = \sum_{j=1}^{m-1} \left(\left(\sum_{i=1}^{j} \overline{\boldsymbol{A}}_i \right) \left((1-\eta)\boldsymbol{F}_{t_{n+1}} + (2\eta-1)\boldsymbol{F}_{t_n} - \eta \boldsymbol{F}_{t_{n-1}} - \Delta h \boldsymbol{K} \boldsymbol{v}_{t_0} - \left(\frac{-\mu}{\gamma} \right)^{n-1} \boldsymbol{\eta}\, \boldsymbol{a}_{t_0} \right) \right) \tag{67b}$$

$$\Delta \boldsymbol{V}_2 = \left(\sum_{i=1}^{m} \boldsymbol{A}_i \right) \left(\eta \boldsymbol{F}_{t_0} + (1-\eta)\boldsymbol{F}_{t_1} - \boldsymbol{K} \left(\boldsymbol{u}_{t_0} + (1-\eta)\Delta h \boldsymbol{v}_{t_0} \right) - \overline{\boldsymbol{R}}^{*} \boldsymbol{a}_{t_0} - \boldsymbol{L}^T \boldsymbol{\Lambda}_{t_0} \right) \tag{67c}$$

$$\Delta \boldsymbol{V}_3 = \left(\sum_{i=1}^{m} (m+1-i)\overline{\boldsymbol{A}}_i - \eta \sum_{i=1}^{m} \overline{\boldsymbol{A}}_i \right) \boldsymbol{L}^T \Delta \boldsymbol{\Lambda} \tag{67d}$$

5.2 | Calculation of the interface link force

For an interface, interconnecting with two subdomains, as shown in Figure 2, the velocity continuity condition (Equation (29)) is used to couple the two subdomains, and the linear interpolation is employed to calculate the intermediated link forces (Equation 16) at time sub-steps. Using Equation (67), velocity increments of the two subdomains over ΔT are solved as follows:

$$\Delta \boldsymbol{V}^A = \Delta \boldsymbol{V}_1^A + \Delta \boldsymbol{V}_2^A + \Delta \boldsymbol{V}_3^A \tag{68a}$$

$$\Delta \boldsymbol{V}^B = \Delta \boldsymbol{V}_1^B + \Delta \boldsymbol{V}_2^B + \Delta \boldsymbol{V}_3^B \tag{68b}$$

Substituting the two velocity increments into the continuity condition Equation (29), one has:

$$\boldsymbol{L}_A\left(\Delta \boldsymbol{V}_1^A + \Delta \boldsymbol{V}_2^A\right) + \boldsymbol{L}_B\left(\Delta \boldsymbol{V}_1^B + \Delta \boldsymbol{V}_2^B\right) = \begin{pmatrix} \boldsymbol{L}_A\left(\sum_{i=1}^{m_a}(m_a+1-i)\overline{\boldsymbol{A}}_i^A - \eta_a\sum_{i=1}^{m_a}\overline{\boldsymbol{A}}_i^A\right)\boldsymbol{L}_A^T/m_a + \\ \boldsymbol{L}_B\left(\sum_{i=1}^{m_b}(m_b+1-i)\overline{\boldsymbol{A}}_i^B - \eta_b\sum_{i=1}^{m_b}\overline{\boldsymbol{A}}_i^B\right)\boldsymbol{L}_B^T/m_b \end{pmatrix}\Delta\boldsymbol{\Lambda}^{A\cdot B} \tag{69}$$

The total link force over the system time step is calculated by the matrix division operation (i.e., \) as follows:

$$\Delta\boldsymbol{\Lambda}^{A\cdot B} = \boldsymbol{H}_2 \backslash \boldsymbol{DV}_2 \tag{70}$$

where coefficients matrices are:

$$\boldsymbol{H}_2 = \begin{pmatrix} \boldsymbol{L}_A\left(\sum_{i=1}^{m_a}(m_a+1-i)\overline{\boldsymbol{A}}_i^A - \eta_a\sum_{i=1}^{m_a}\overline{\boldsymbol{A}}_i^A\right)\boldsymbol{L}_A^T/m_a + \\ \boldsymbol{L}_B\left(\sum_{i=1}^{m_b}(m_b+1-i)\overline{\boldsymbol{A}}_i^B - \eta_b\sum_{i=1}^{m_b}\overline{\boldsymbol{A}}_i^B\right)\boldsymbol{L}_B^T/m_b \end{pmatrix} \tag{71a}$$

$$\boldsymbol{DV}_2 = \boldsymbol{L}_A\left(\Delta \boldsymbol{V}_1^A + \Delta \boldsymbol{V}_2^A\right) + \boldsymbol{L}_B\left(\Delta \boldsymbol{V}_1^B + \Delta \boldsymbol{V}_2^B\right) \tag{71b}$$

So far, link forces are solved, two interconnected subdomains are decomposed into independent computational subdomains; two independent substructures can be coupled into an entire domain; and the number of subdomains can easily extend to multi-subdomains.

5.3 | Implementation of Generalized-α

Substituting the solved link forces (Equation (70)) into the coupling equations (Equation (14)), the decoupling subdomains with different time steps can be solved independently and efficiently. Using dynamic Equation (28), decoupling equations are written as follows:

$$\begin{cases} \overline{\boldsymbol{K}}_*^1\Delta\boldsymbol{v}_{t_i}^1 = \mathbb{F}_{t_i}^1 - \mathbb{L}_1^T\Delta\mathfrak{R}_{t_i}^1 & \forall t_i \in \{1, m_1\} \\ \vdots & \\ \overline{\boldsymbol{K}}_*^k\Delta\boldsymbol{v}_{t_k}^k = \mathbb{F}_{t_k}^k - \mathbb{L}_k^T\Delta\mathfrak{R}_{t_k}^k & \forall t_k \in \{1, m_k\} \\ \vdots & \\ \overline{\boldsymbol{K}}_*^S\Delta\boldsymbol{v}_{t_S}^S = \mathbb{F}_{t_S}^S - \mathbb{L}_S^T\Delta\mathfrak{R}_{t_S}^S & \forall t_S \in \{1, m_S\} \end{cases} \tag{72}$$

where the intermediated link forces $\boldsymbol{\Lambda}_j$ can be solved by using Equation (16). It is important to note that for all integration methods with a single time step, only the Newmark method can provide the strict energy stability demonstration.[32] Therefore, numerical analyses are performed to verify the energy stability characteristics of the proposed method with NG schemes. The implementation of the proposed method with NG can similarly refer to Table A1.

6 | REPRESENTATIVE EXAMPLES AND DEMONSTRATION

Two representative numerical examples are adopted to investigate the properties of the proposed method. Specifically, a single DOF oscillator with an analytical solution is used to discuss the energy dissipation and accuracy properties, and a sandwich beam subjected to high-frequency impact loadings is employed to study the accuracy, dissipation property, and computational efficiency of the proposed method in terms of a complex dynamic system.

6.1 | Single DOF system with an analytical solution

An oscillator split into four parts, that is, subdomain A (Sub_A), Sub_B, Sub_C, and Sub_D, is here discussed, as shown in Figure 3. The dynamic equation and initial conditions are:

$$\begin{aligned} &\overline{m}a(t) + ku(t) = 0 \\ &u(0) = 1, \qquad v(0) = 0 \end{aligned} \tag{73}$$

where $a(t)$ and $u(t)$ refer to the acceleration and displacement of the entire oscillator, respectively. The analytical solution is $u(t) = \cos(\omega t)$, where ω is the natural frequency of the oscillator. The initial mechanical energy and pseudo-energy of the oscillator are $W_0 = 146{,}300$ and $E_0 = 1.0701845 \times 10^{16}$, respectively. In this example, the interface mechanical energy and pseudo-energy are discussed first. Subsequently, the proposed method's accuracy is studied by varying time-step sizes, time-step ratios, and algorithmic parameters of subdomains.

6.1.1 | Investigation of energy dissipation

To study the properties of the mechanical energy and pseudo-energy of the proposed method, three cases are discussed, whose computational parameters are given in Table 1. In particular, Case I: to study the influence of time step ratios on the system energy dissipation, different time-step sizes of subdomains are selected according to the frequency content of subdomains. Case II: to explore the effect of time-step sizes, the time-step sizes of Case I are increased by 10 times and maintained at the same ratio. Case III: the same time-step size is set in all subdomains for comparison. For convenience, the reduced angular frequency ($\Phi = 2\pi\, \Delta t/\Delta T$) is employed in the analysis.[20,21] $\Phi_B = 0.1$ (i.e., $\Delta t/\Delta T = 0.016$) is set as the critical ratio of the time step size/the system period ($\Delta t/\Delta T$) to accurately compute the system responses, and the critical time step Δt is thus limited to 3.6974×10^{-7} s. More information on the critical time step can be found in References 20,21.

Interface mechanical energy

To study the properties of the interface mechanical energy under different time step ratios, the proposed method (including Newmark scheme and six NG schemes; $\rho = 1$) is used to calculate the coupling oscillator with different time step ratios, and the interface mechanical energy of Cases I and III is presented in Figure 4. It is worth noting that the six schemes of

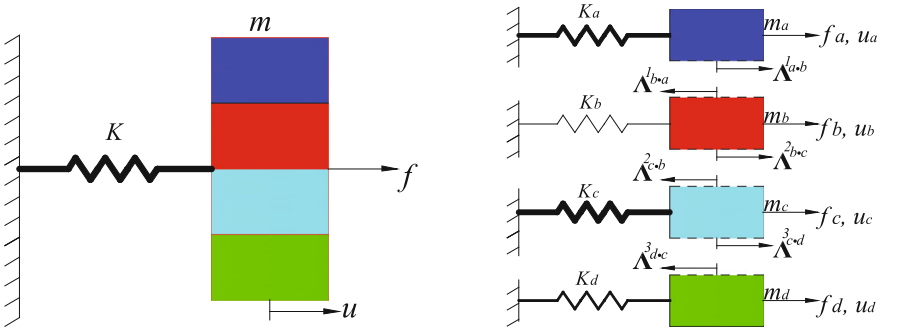

(A) A domain with different properties (B) Partitioned computational subdomains

FIGURE 3 Complex oscillator split into four subdomains (m_a, m_b, m_c, m_d) and (K_a, K_b, K_c, K_d) are the masses and stiffness of the four subdomains, respectively

TABLE 1 Calculation parameters of the split oscillator

Items	Mass $\times 10^{-6}$	Stiffness $\times 10^{3}$	Time sub-steps Case I $\times 10^{-8}$	Case II $\times 10^{-7}$	Case III $\times 10^{-6}$	Ratios	Parameters (γ, β)
Sub_A	1.0	40	0.5	0.5	1.0	20	(1/2, 1/4)
Sub_B	1.0	0.1	10	10	1.0	1	(1/2, 1/4)
Sub_C	1.0	250	0.2	0.2	1.0	50	(1/2, 1/4)
Sub_D	1.0	2.5	2.0	2.0	1.0	5	(1/2, 1/4)
Entire domain	4.0	292.6	$\Delta t = 3.6974 \times 10^{-7}$			27.05	(1/2, 1/4)

Note: Note that algorithmic parameters of Newmark are given in brackets as (γ, β); and the calculation time is 0.01 s.

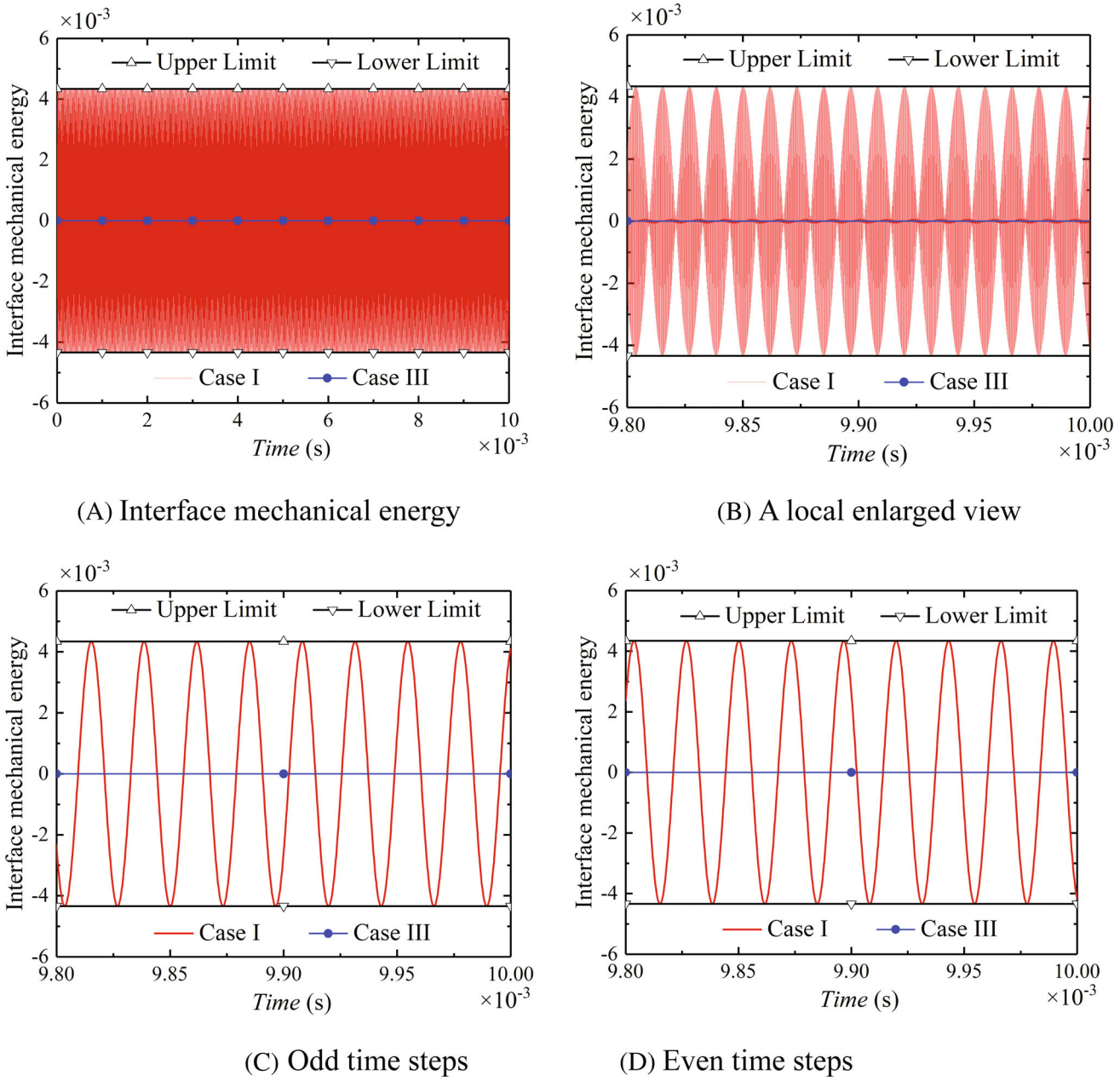

FIGURE 4 Interface mechanical energy under different time step ratios

NG method have the same displacement and velocity integration scheme as Newmark scheme with (1/2, 1/4) when $\rho = 1$, and thus Equation (56) can be used to calculate the interface mechanical energy of NG schemes; only case numbers are marked in the figure because seven energy curves are overlapped for all cases; and upper limit and lower limit of the interface mechanical energy are 0.004339363 and −0.004339363, respectively. Due to the same time step size and algorithmic parameters ($\beta = 1$) used in all subdomains of Case III, the interface mechanical energy is always zero, which can also be confirmed by Equation (56). To observe the results of Case I, an enlarged view from 0.98×10^{-2} s to 1×10^{-2} s is depicted in Figure 4B. It is shown that the interface mechanical energy generated by link forces is extremely small compared with the initial mechanical energy ($W_0 = 146{,}300$), and the periodic oscillation property is observed. To explore the periodicity of the energy oscillation, the interface mechanical energy is divided into two continuous periodic oscillations according to the parity of time steps, which are shown in Figures 4C,D. The energy amplitude is not amplified and minified within the entire calculation time for the entire system. Therefore, for subdomains with different time step ratios (i.e., Case I), zero dissipation of mechanical energy is ensured in the dynamic computation, but a small part of the system mechanical energy is transferred as the interface mechanical energy with the periodic oscillation property. In addition, for subdomains with the same time step sizes and algorithmic parameters $\beta = 1/4$ (i.e., Case III), the system mechanical energy is conservative, and zero mechanical energy is ensured at the interface of interconnected subdomains.

To investigate the effect of time-step sizes on the interface mechanical energy, for Case II and Case III, curves of the interface mechanical energy and its enlarged view are depicted in Figure 5. Note that the time-step size of Sub_B in Case II (i.e., $\Delta t_b = 1.0 \times 10^{-6}$ ($\Phi_B = 0.27$)) is larger than the critical time-step size ($\Phi_B = 0.1$), which leads to large period elongations.[36] Namely, interface link forces calculated by both Newmark schemes and NG schemes ($\rho = 1$) are coarse.

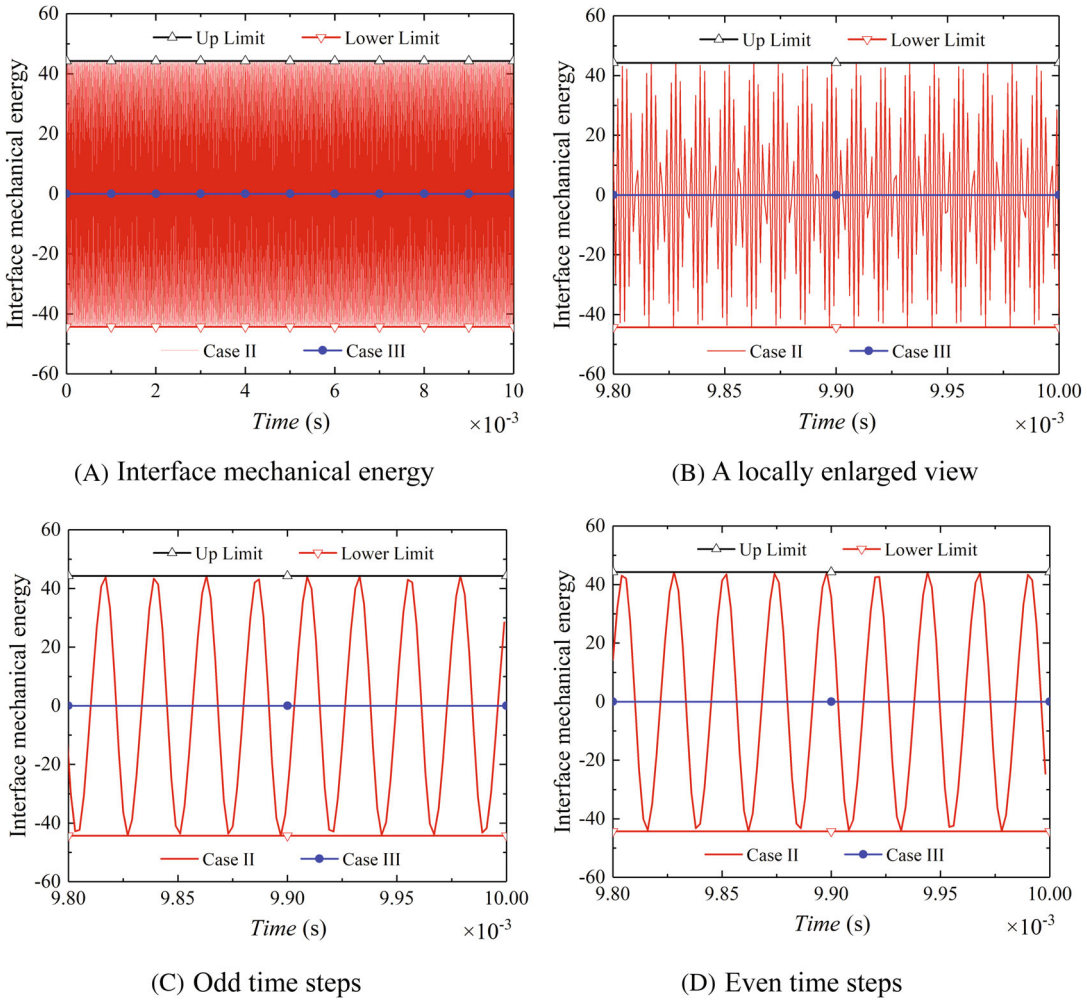

FIGURE 5 Interface mechanical energy under different time-step sizes solved by using the proposed method including Newmark scheme and NG schemes ($\rho = 1$)

Therefore, the amplitude of the interface energy is amplified significantly compared with that of Case I (i.e., the time step sizes of subdomains can be used to adjust the interface mechanical energy), but it is still extremely small compared with W_0. Moreover, according to the parity of time steps, the interface mechanical energy is also divided into two continuous periodic oscillations, which are plotted in Figure 5B,C, and periodic oscillation is still observed within the entire calculation time. Namely, zero dissipation and the periodic oscillation of the interface mechanical energy can be observed in dynamic computation.

Interface pseudo-energy

The theoretical interface pseudo-energy under all cases should be equal to zero according to Equation (51). However, the initial input pseudo-energy is $E_0 = 1.0701845 \times 10^{16}$, and the pseudo-energy amplitude is close to 1.8887×10^{14} for the four subdomains. Therefore, a tiny pseudo-energy is observed in numerical results due to floating-point operation errors, and it is accumulated and amplified by the system time step (see Equation (50)). To accurately calculate the pseudo-energy, the rational number operations are conducted, and zero dissipation of the interface pseudo-energy is found in the numerical results. Therefore, the proposed method features the pseudo-energy conservation property.

Comparison with existing methods

It is not easy to extend the application of the four-subdomain system to the existing multi-time step methods.[13–17,36] Therefore, the oscillator split into two subdomains is investigated to compare with the existing multi-time step methods. Specifically, the mass and stiffness of Sub_A and Sub_B are $m_a = m_b = 1 \times 10^{-6}$ and $K_a = K_b = 1 \times 10^4$, respectively; the time steps for Sub_A and Sub_B are 1×10^{-6} and 1×10^{-7}, respectively; the simulation time is 0.01 s; the pseudo-energy of NG schemes ($\rho = 0.5$) is analogously calculated by using Equation (50); and the initially imported pseudo-energy is $\Delta E_{initial,n} = 1 \times 10^{14}$. Accumulated interface pseudo-energy curves are plotted in Figure 6. It is shown that the accumulated pseudo-energy gradually dissipates with time and approaches the initially imported pseudo-energy at the end time (0.01 s) for GC and BGC_Micro. On the contrary, the pseudo-energy is zero for the proposed method with different schemes, BGC_Macro, and PH. Moreover, the pseudo-energy of the proposed method can also be directly derived from Equation (50). Note that to avoid floating-point operation errors, rational number operations should be chosen in the computation. Therefore, the proposed method features the interface pseudo-energy conservation property.

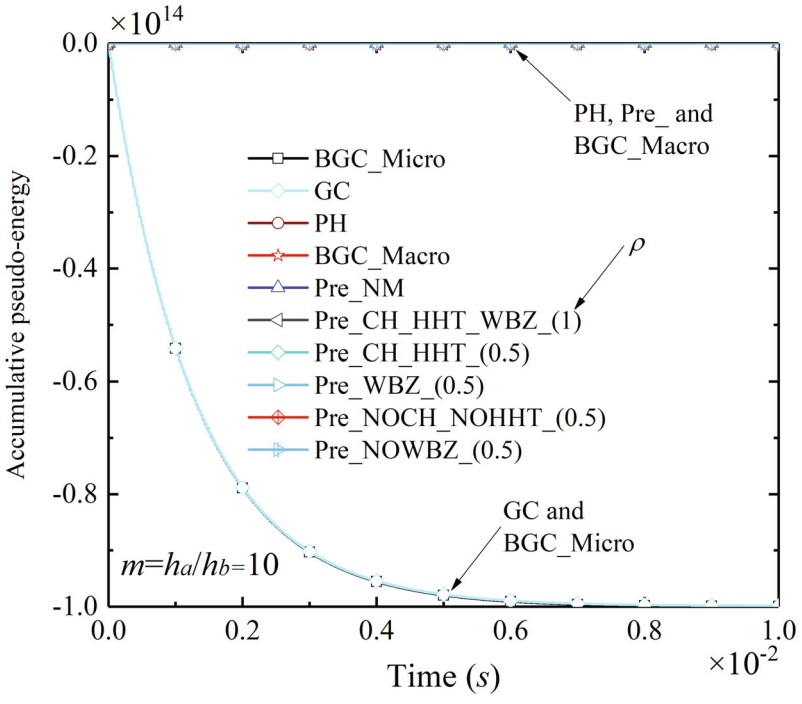

FIGURE 6 Pseudo-energy of various coupling methods ($m = 10$). Pre_() denotes the **Pre**sented method with specified schemes such as Pre_NM represents Newmark scheme; the number in brackets refers to ρ; and CH and HHT have the same schemes when $\rho = 0.5$, which are written as Pre_CH_HHT

6.1.2 | Discussion of accuracy

The accumulated absolute error[1] of the coupling oscillator is calculated to assess the accuracy property of the proposed method considering varying integration schemes.

$$Error_k = \sqrt{e_k / e_{theo}} \qquad k = a, b, c, d \tag{74a}$$

$$\tilde{e}_k = \sum_{i=1}^{N} \left(Wk_{simu}^{m_k*(i-1)+1} - W_{theo}^{i} \right)^2, \qquad \tilde{e}_{theo} = \sum_{i=1}^{N} \left(W_{theo}^{i} \right)^2 \qquad i = \{1, 2, , , N\} \tag{74b}$$

where $\tilde{e}_k$ and $\tilde{e}_{theo}$ refer to the accumulated absolute errors of numerical solutions and theoretical solutions, respectively; Wk_{simu} and W_{theo} indicate the numerical solutions and theoretical solutions of each subdomain, respectively; and N and m_k denote the numbers of the system time step and time sub-steps of the kth subdomain within the calculation time of 0.001 s, respectively. Various time-step sizes and algorithmic parameters of the proposed method are employed in the calculation below to explore the accuracy property under different scenarios.

6.1.3 | Different time-step sizes

Computational conditions

The time-step sizes of Sub_A, Sub_B, Sub_C, and Sub_D are, respectively, $\Delta h_B = \Phi_B$, $\Delta h_A = \Delta h_B/20$, $\Delta h_C = \Delta h_B/50$, and $\Delta h_D = \Delta h_B/5$; the range of Φ_B from 0.01 to 0.1 is examined in the computation; CH, HHT, WBZ, and Newmark with the macro time step are used to calculate the entire oscillator (i.e., Figure 3A) for comparison. The results of all subdomains have similar patterns, and the results of Sub_B have relatively large absolute errors due to the used macro time step, and the error curves of Sub_B under different methods are thus shown in Figure 7. It is shown that the absolute errors of all quantities (i.e., displacement, velocity, and acceleration) increase with the time-step size (Φ_B). Except for Newmark method, the accumulated absolute errors of all quantities for the proposed method decrease with the increase of the ρ as Pre_CH-WBZ (0) has the largest error. The error curves of the integration schemes with $\rho = 1$ (i.e., Pre_CH and Pre_HHT-WBZ) are overlapped. Due to the realization of the small-time step at subdomains, errors from the proposed method are smaller than errors from CH, HHT, and WBZ. Compared with Newmark method with the second-order accuracy, the proposed method maintains the second-order accuracy in terms of displacement and velocity results. For $\rho = 1$ (i.e., Pre_CH and Pre_HHT-WBZ), the acceleration of the proposed method has the second-order accuracy, and the acceleration of the proposed method only has the first-order accuracy when $\rho \neq 1$ such as Pre_CH-HHT (0.5). Thus, both the time-step size and spectral radius can be used to adjust the accuracy of the proposed method.

6.1.4 | Various algorithmic parameters

To investigate the accuracy properties of the proposed method under different algorithmic parameters (i.e., β and ρ), based on the following computational conditions, the error curves of Sub_B with the macro time step are presented in Figure 8. *Computational conditions*: The time-step sizes of Sub_A, Sub_B, Sub_C, and Sub_D are, respectively, $\Delta h_B = \Phi_B = 0.1$, $\Delta h_A = \Delta h_B/20$, $\Delta h_C = \Delta h_B/10$, and $\Delta h_D = h_B/5$; corresponding time step ratios are (20, 1, 10, 5); algorithmic parameters of the four subdomains are given in Table 2; and CH, HHT, WBZ, and Newmark method with the macro time step are used to calculate the entire oscillator for comparison. It is shown that since more accurate link forces are solved in subdomains with the micro time-step size by the proposed method with Newmark scheme, the results of all calculation quantities from the proposed method with Newmark scheme (i.e., Pre_NM) have higher accuracy than that from Newmark method with parameters, except for ($\beta = 1/12.8$–$1/11.2$). Similar observations can be found in other algorithm pairs such as Pre_CH and CH. Moreover, except for Newmark method, the accumulated absolute errors of all quantities decrease with the increase of the parameters β and ρ. Therefore, decreasing the time step sizes of subdomains can improve the computational accuracy of the coupling system, and the accuracy of all subdomains can be adjusted by using their own integration parameters.

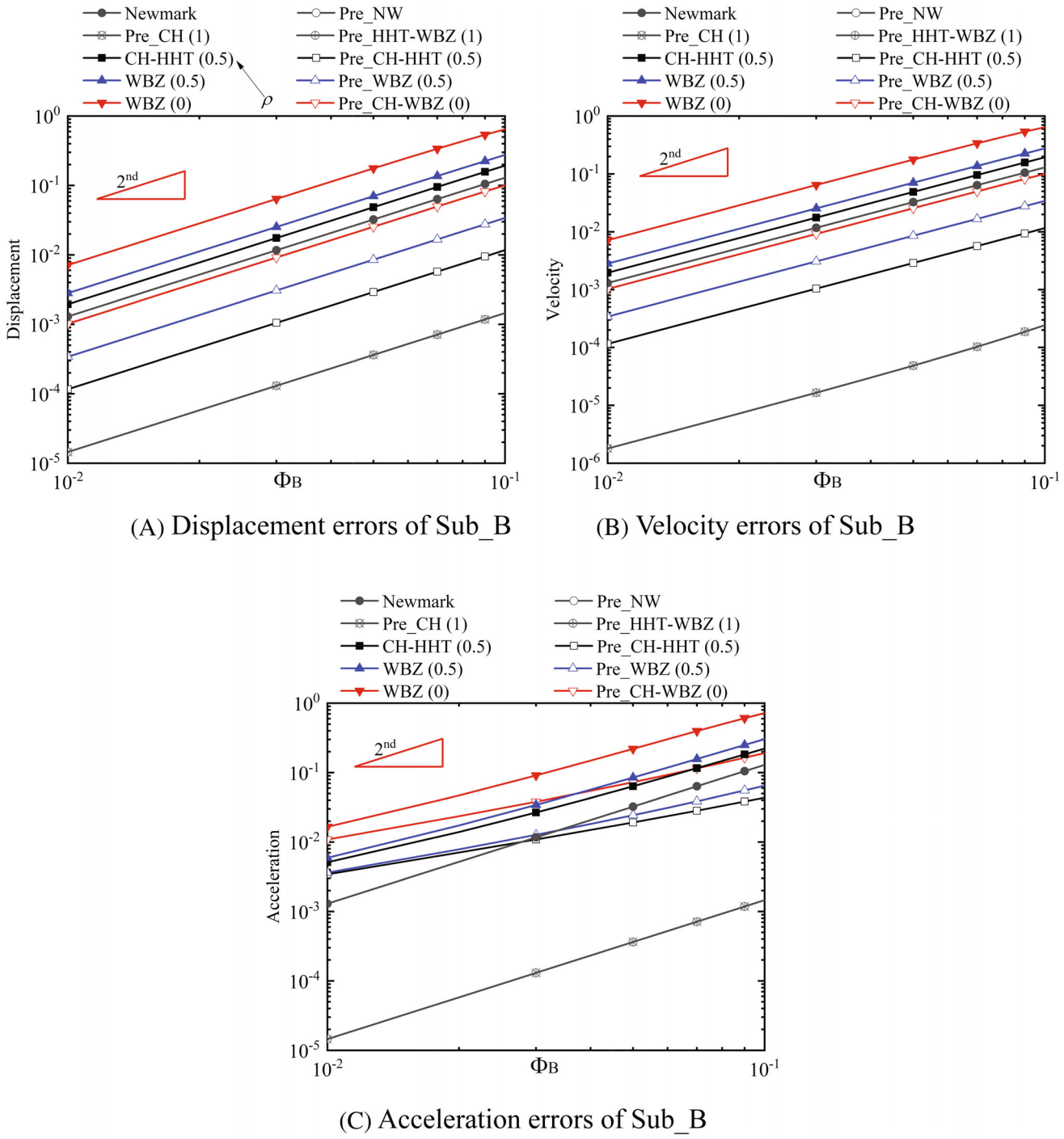

FIGURE 7 Error curves of integration methods considering different time-step sizes

6.1.5 | Comparison with existing methods

To compare with the accuracy of the existing coupling methods, based on the following computational conditions, the oscillator with two subdomains (i.e., Sub_A and Sub_B) is employed to study the accuracy properties of the proposed method under different algorithmic parameters β by contrast. *Computational conditions*: The time steps are $\Delta h_A = 10^{-6}$ s and $\Delta h = \Delta h_A/20$; corresponding mass and stiffness information of the two subdomains is given in Table 1; algorithmic parameters ($\gamma = 1/2$ and various β) and ($\gamma = 1/2$ and $\beta = 1/4$) of the existing methods with Newmark scheme (i.e., PH, BGC_Macro, BGC_Micro, and GC) are employed to solve responses of Sub_A and Sub_B, respectively; and Newmark

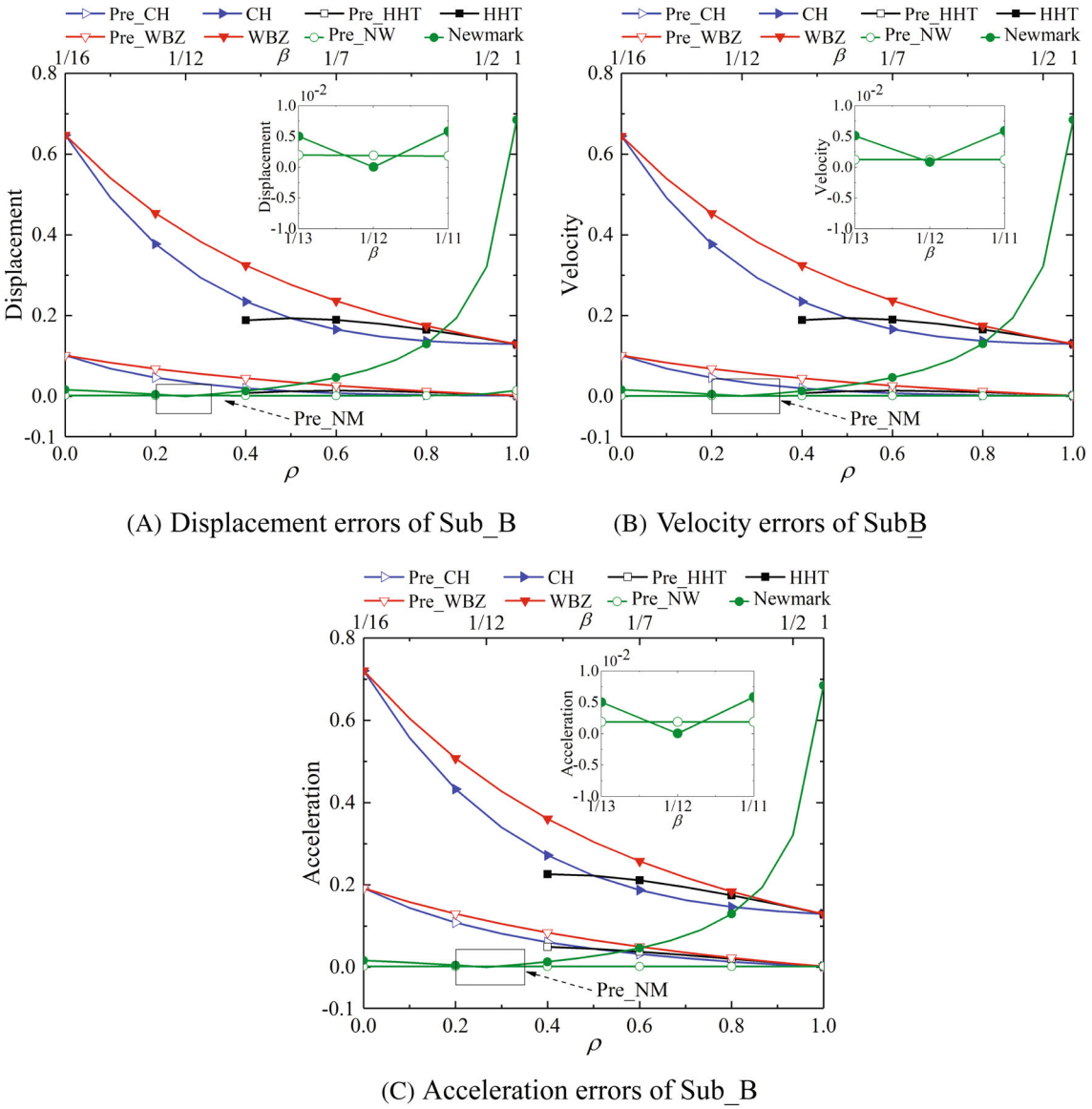

FIGURE 8 Error curves of integration methods considering various algorithmic parameters (β or ρ). Note that the upper abscissa and lower abscissa indicate the varying parameter β (Pre_NM) and ρ (Pre_NG), respectively

TABLE 2 Algorithmic parameters of the four subdomains

Items	Pre_CH	Pre_HHT	Pre_WBZ	Pre_NW	CH/HHT/WBZ/Newmark
Sub_A and Sub_C	ρ	ρ	ρ	(1/2, β)	ρ *or* (1/2, β)
Sub_B and Sub_D	$\rho=1$	$\rho=1$	$\rho=1$	(1/2, 1/4)	$\rho=1$ i.e., (1/2, 1/4)

method with ($\gamma=1/2$ and various β) and $\Delta h=10^{-6}$ s is used to calculate the entire oscillator for comparison. Due to the employed macro time step, error curves of Sub_A under various β are shown in Figure 9.

It is shown that Newmark with parameters ($\beta=1/12.8$–$1/11.2$) has higher accuracy than that of the energy-conservative coupling methods (i.e., PH, BGC_Macro, and Pre_NM). Furthermore, although more accurate link forces are solved in Sub_B with a micro time step, the third-order accuracy cannot be obtained for the energy-conservative coupling methods. Accuracy for the energy-conservative coupling methods gradually increases from $\beta=1/12$ to the two sides. When Newmark scheme is used in the analysis for the two-subdomain scenario, the proposed method exactly regresses to PH and BGC_Macro.

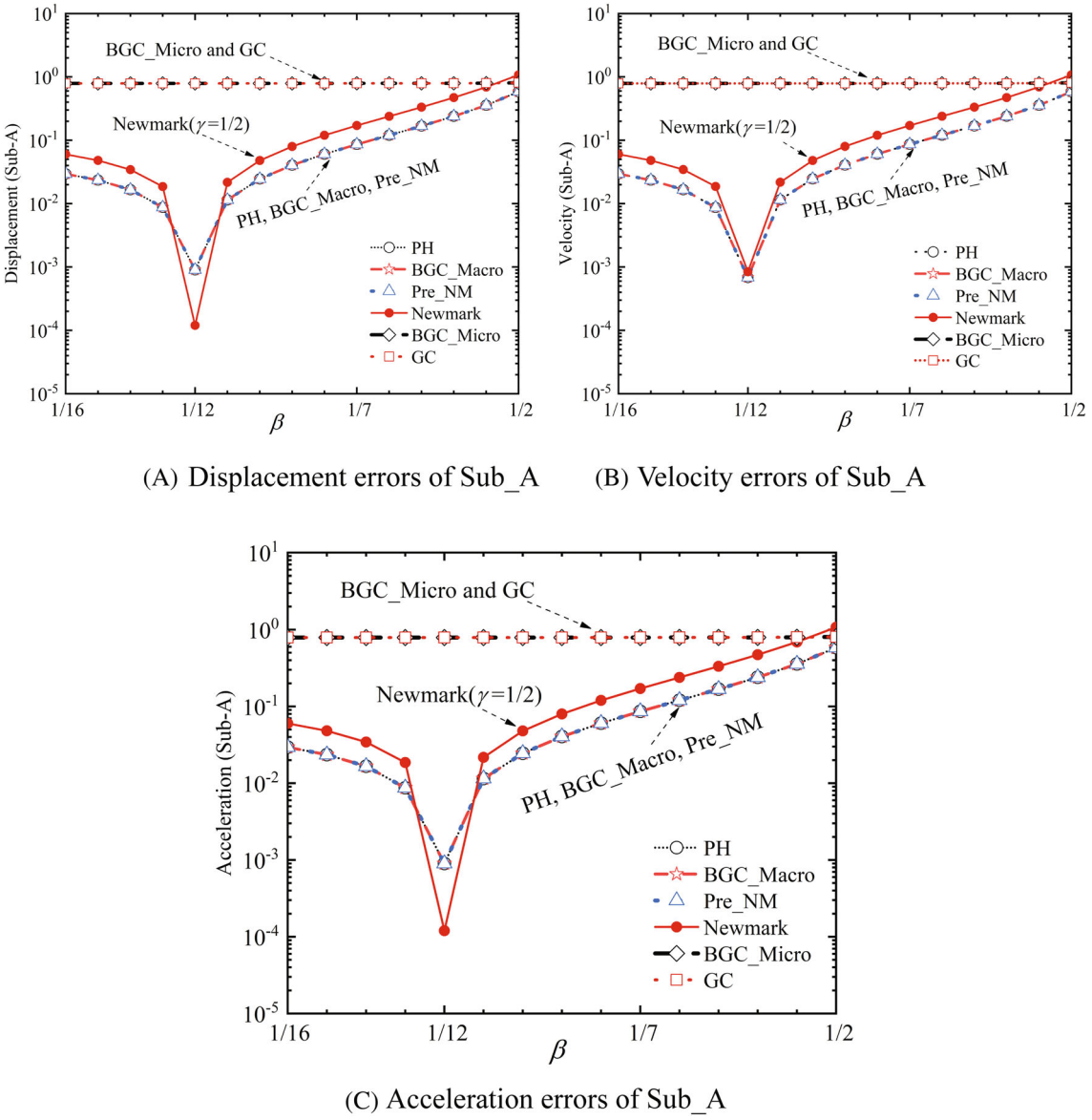

(A) Displacement errors of Sub_A (B) Velocity errors of Sub_A

(C) Acceleration errors of Sub_A

FIGURE 9 Error curves of integration methods considering various algorithmic parameters β ($\rho = 1$ and $m = 20$)

6.2 | Sandwich beam subjected to high-frequency impacts

A sandwich beam with multiple local damages, as shown in Figure 10, is used to investigate the computational accuracy, energy property, and efficiency of the proposed method in terms of complex problems. The dimension information of the beam and the notch is given in Figure 10A,B, respectively. The material parameters for material 1 are: Young modulus = 150 GPa, density = 6300 kg/m^3, and Poisson's parameter = 0.3. The material parameters for material 2 are: Young modulus = 270 GPa, density = 9100 kg/m^3, and Poisson's parameter = 0.3. Loads applied to the beam in the vertical and horizontal directions are:

$$\begin{cases} F_v(t) = 2P\sin(\omega t) \\ F_h(t) = 2P\sin(\omega t) \end{cases} \quad P = 1e5, \quad \omega = 10\pi \tag{75}$$

where P and ω are the amplitude and the frequency of applied loads in vertical and horizontal directions, respectively. Considering the symmetry of the beam and vertical loads and the anti-symmetry of the horizontal loads, the half structure is modelled in this study. Two models are built in the analysis for comparison. In particular, an entire model with 2524

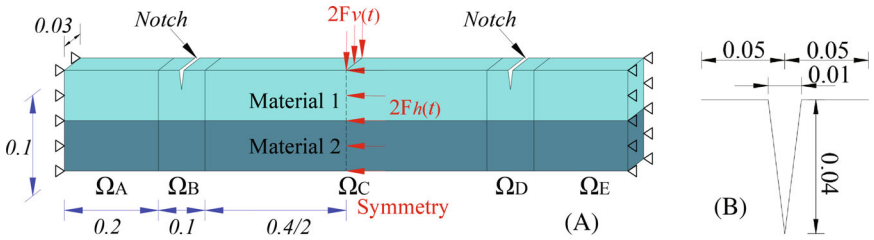

FIGURE 10 A damaged sandwich beam (Unit: m). (A) Sandwich beam subjected to high-frequency impact loads and its dimension, and (B) Dimension of the notch

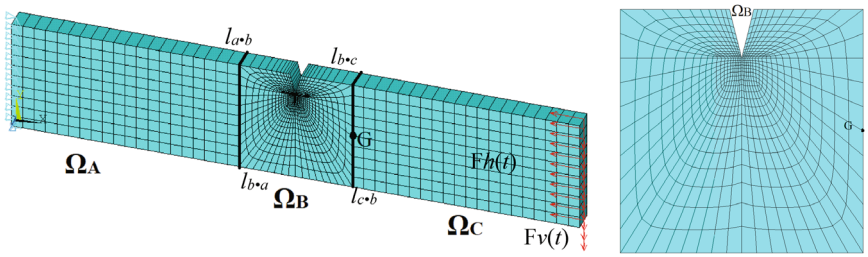

FIGURE 11 Finite element analytical model of the beam

TABLE 3 Time-step sizes of different cases

Item	Case 1	Case 2	Case 3	Case 4	Case 5	Ratios
Sub_A	$(5\times10^{-7}, 1/4)$	$(5\times10^{-7}, 1/3)$	$(5\times10^{-7}, 1/4)$	$(5\times10^{-8}, 1/4)$	$(1\times10^{-6}, 1/4)$	50
Sub_B	$(1\times10^{-8}, 1/4)$	$(1\times10^{-8}, 1/3)$	$(1\times10^{-8}, 1/6)$	$(1\times10^{-9}, 1/3)$	$(2\times10^{-8}, 1/4)$	1
Sub_C	$(1\times10^{-7}, 1/4)$	$(1\times10^{-7}, 1/3)$	$(1\times10^{-7}, 2/5)$	$(1\times10^{-8}, 2/5)$	$(2\times10^{-7}, 1/4)$	10
Entire model	$(2\times10^{-9}, 1/4)$					

Note: Note that the first and second numbers in all brackets are the time-step size and algorithmic parameter β, respectively; algorithmic parameter $\gamma = 1/2$ is assumed in all cases to ensure the second order in results; and implicit schemes and explicit schemes are used in Sub_A/C and Sub_B, respectively, that is, hybrid schemes are used in this calculation.

DOFs (i.e., the first model) is solved by using a unique time step, whose results are regarded as the reference values. The second model is composed of three subdomains, as shown in Figure 11. The numbers of DOF for Sub_A, Sub_B, and Sub_C are, respectively, 440, 1666, and 462. It is important to note that the 1st order frequency, the 7th order frequency, and the highest frequency of the steel beam are, respectively, 302.24 Hz, 10015.86 Hz ($\Phi = 0.063$), and 6,090,536 Hz ($\Phi = 38.27$), and a small-time step size is thus required to capture high-frequency responses of the beam. *Five scenarios* of time step sizes are set in the second model as presented in Table 3 to discuss the accuracy, energy, and efficiency of the proposed method. More specifically, two time-step ratios (i.e., 50 and 10) of subdomains are set in all cases of the second model to explore the influence of time step ratios on the accuracy; the same time-step ratios but different algorithmic parameters are employed in Cases 1, 2, and 3 to investigate the effect associated with algorithmic parameters; and the time-step size of Case 3 is decreased by 10 times (i.e., Case 4) and increased by 2 times (i.e., Case 5) to analyze the influence of the time-step size. It is worth noting that the algorithmic parameters of Sub_B in Case 3 is set as 1/6, and the explicit scheme is used in the calculation of Sub_B.

6.2.1 | Investigation of accuracy

Since high-frequency vibrations are observed in the horizontal direction based on the numerical results of the three subdomains, the responses of G point (marked in Figure 11) in the horizontal direction are presented in Figure 12 to assess the accuracy of the high-frequency computation. It is worth noting that displacement responses at the G point,

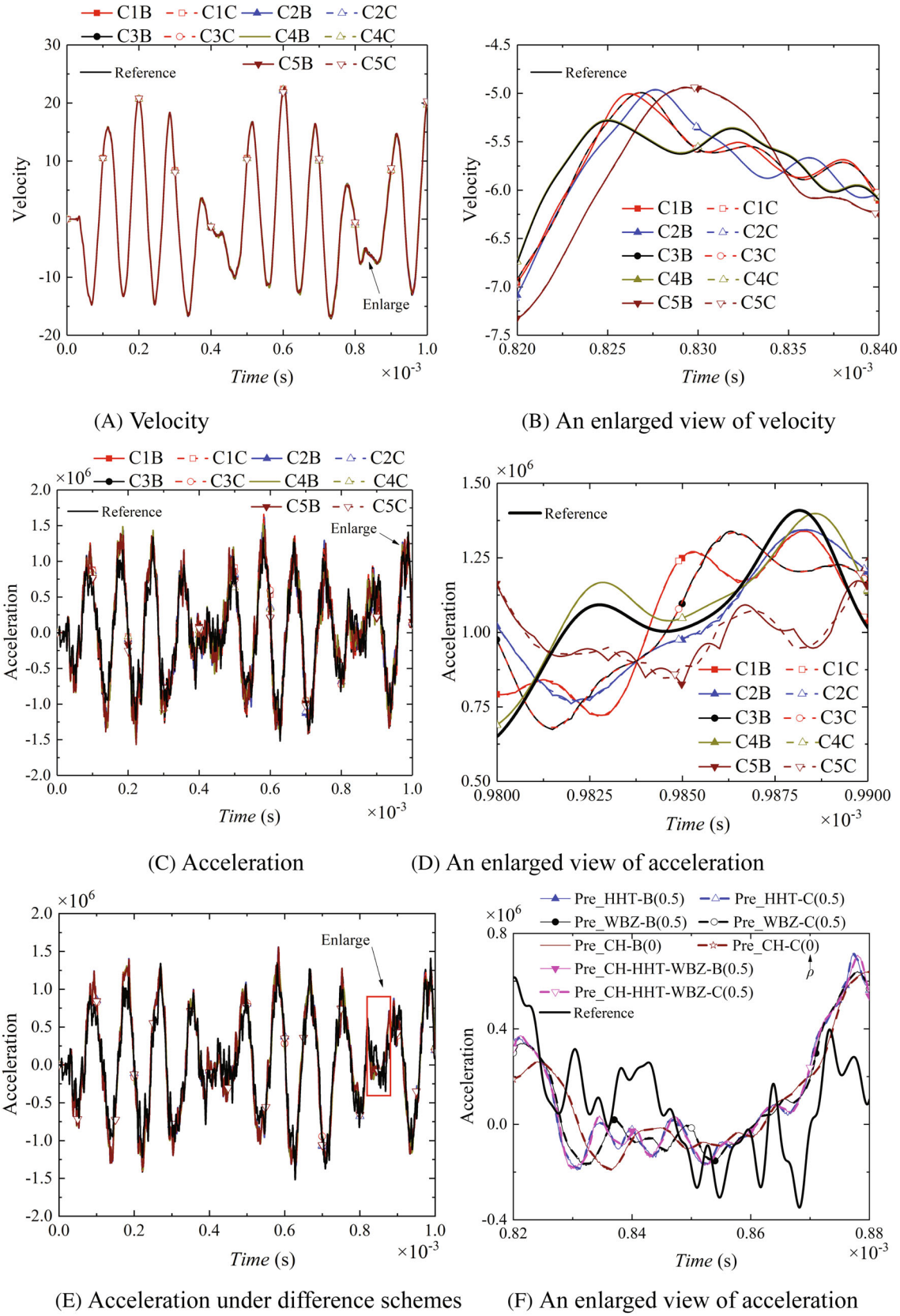

FIGURE 12 Structural responses of the G point considering different cases. For (A–D), the first, second, and third letters in labels mean the 'Case', case number, and subdomain number (Sub_B and Sub_C). Pre_HHT-B in (E, F) is the presented method with three NG schemes considering varying ρ, and B and C are the names of the two subdomains

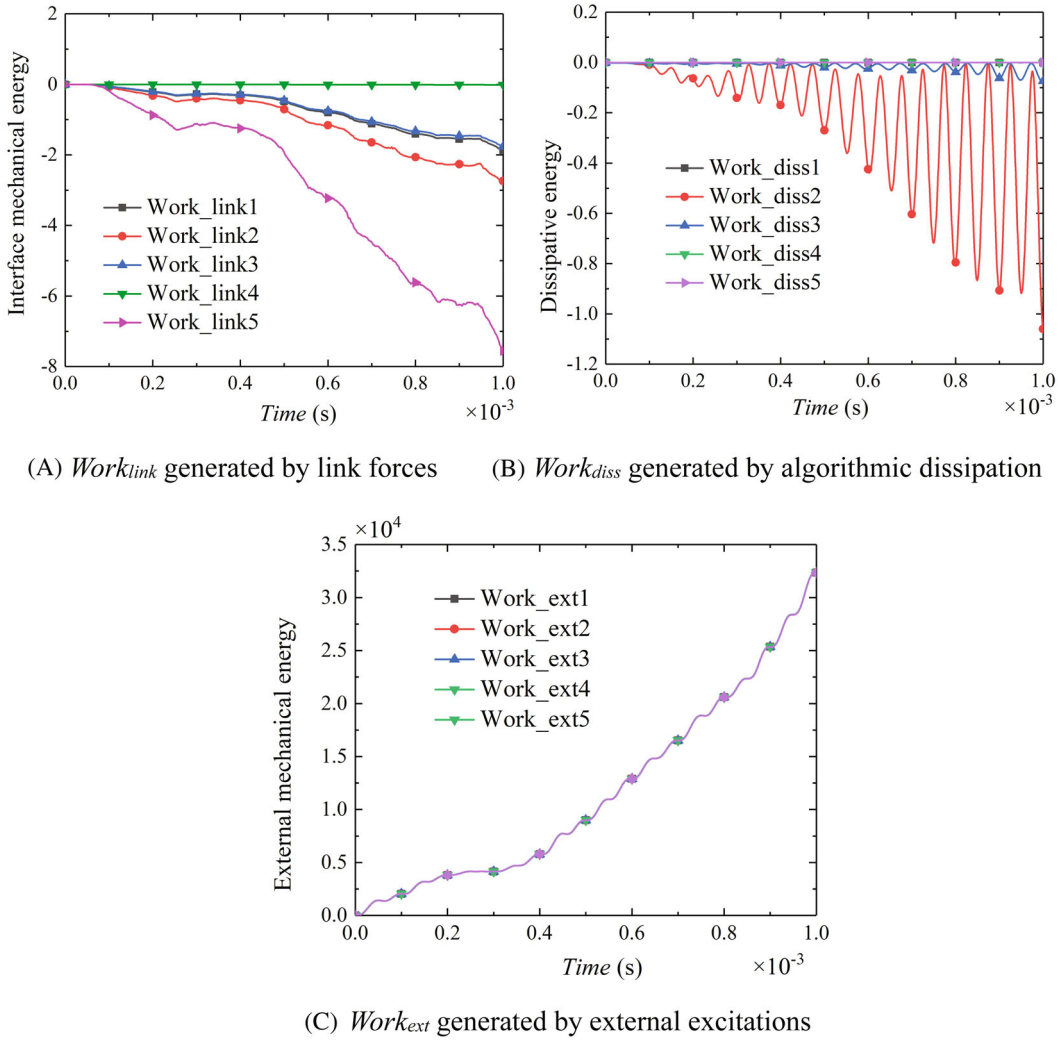

(A) $Work_{link}$ generated by link forces (B) $Work_{diss}$ generated by algorithmic dissipation

(C) $Work_{ext}$ generated by external excitations

FIGURE 13 Accumulated interface mechanical energy under different cases. The case number is labelled at the behind of labels

from Sub B and Sub C, overlap with the reference values for all computational cases. Local high-frequency responses of velocity and acceleration, as marked in Figure 12A,C, are enlarged in Figure 12B,D, respectively. Due to high-frequency vibrations of the steel beam (e.g., the 7th frequency is 10015.86 Hz) and a large time step (1.0×10^{-6}) adopted, inconsistent acceleration responses (see Figure 13E) are captured in Case 5. Except for a slight difference in accelerations in Case 5, all responses at the G point from the two subdomains are overlapped for all cases. Therefore, interconnected subdomains, solved by the proposed method accounting for different parameters and time-step sizes, can be coupled very well. Moreover, due to the relatively small time-steps used in Case 4, responses of displacements and velocities overlap with the reference results. Although the same time-step sizes are employed in Cases 1, 2, and 3, slight differences are observed in the results due to different algorithmic dissipations. With the decrease of the time-step sizes (from Case 5 to Case 3 to Case 4), responses for all cases gradually approach the reference values, as shown in Figures 12B,D. Therefore, both the time-step size and algorithmic parameters can be used to adjust the accuracy of the proposed method.

Moreover, to explore the computational accuracy of the proposed method considering various NG schemes, Case 1 is calculated, that is, different time step sizes and time step ratios are discussed in the analysis. High-frequency responses of accelerations at G point and its enlarged view are given in Figure 12E,F, respectively. Four combined schemes are investigated as Pre_HHT_B(0.5) denotes the responses of B subdomain at G point considering $\rho = 0.5$, and HHT represents the same schemes used in three subdomains. It is shown that all results can have a good match with the reference value, except for the high-frequency region (see Figure 12E); and for all combined schemes, responses of two subdomains at G point overlap (see Figure 12F). Therefore, considering various time-step sizes and ratios, algorithmic parameters, and schemes, the proposed method with NG can obtain desirable results.

6.2.2 | Analysis of system energy

To explore the characteristics of accumulated mechanical energy under different time-step sizes and algorithmic parameters, based on the obtained numerical results of the three subdomains, each part of accumulated interface mechanical energy (see Equation 55) is separately given in Figure 13. Some observations on $Work_{link}$ are found: it gradually increases with the increasing time-step size such as Cases 4, 3, and 5; and it is almost equal to zero for Case 4 with the smallest time step. Therefore, time-step sizes of subdomains can be used to adjust the interface mechanical energy generated by link forces. In addition, for the cases with the same time-step sizes and different algorithmic parameters such as Cases 1, 2, and 3, $Work_{link}$ is slightly different. Thus, algorithmic parameters have a slight influence on $Work_{link}$. Although Newmark schemes with parameters (1/2, 1/4) are used in all subdomains of Case 1, $Work_{link}$ still exists in interfaces due to the different time-step sizes. Some similar conclusions are found in $Work_{diss}$, as depicted in Figure 13B. Specifically, the time-step size can be employed to effectively adjust dissipative energy, as shown in Case 4. For Newmark scheme with parameters (1/2, 1/4), tiny dissipative energy $Work_{diss}$ is still observed in Cases 1 and 5. $Work_{ext}$ shown in Figure 13C is almost equal to the total energy ($Work$). In addition, the theoretical pseudo-energy does not exist in interfaces, but a tiny pseudo-energy is observed at interfaces due to floating-point operation errors.

6.2.3 | Evaluation of efficiency

To assess the computational efficiency of the proposed method, two subdomains (i.e., Sub_A and Sub_B) are combined into a new computational domain by using the reconstructed interfaces (i.e., $l_{a\bullet c}$ and $l_{c\bullet a}$). The time-step sizes of Sub_A and Sub_B are, respectively, 2e-7 s and 1e-7 s. The computational efficiency of two element sizes is investigated. In particular, element size 1 is identical to that of the model in Figure 12, and half of the element size 1 is set as size 2. Based on the discussion of the computational efficiency, as shown in Figure 9, Pre_NM, BGC_Macro, and PH have the same computational accuracy, and they have higher accuracy than BGC_Micro and GC. Two parameter combinations are analyzed in this study, (i.e., Pre_NM_c1 and Pre_NM_c2). The five methods are here compared in the analysis. To observe the variation of the computational cost with the simulation time, given the element size 1, Figure 14A shows the elapsed times of various computational methods under 10 kinds of simulation time. Figure 14B presents the elapsed times of various computational methods considering two kinds of element sizes and the simulation time of 0.02 s. For the existing MMTS methods, all subdomain vibrations of the existing MMTS methods are split into free vibrations and link vibrations (i.e., twice complete vibrations are performed at each time step). Moreover, the time-consuming border programme is employed in the computational process, especially for the subdomains with micro time steps. Hence, the existing methods are not dominant in computational efficiency. Conversely, once the calculation is performed at each time step of all

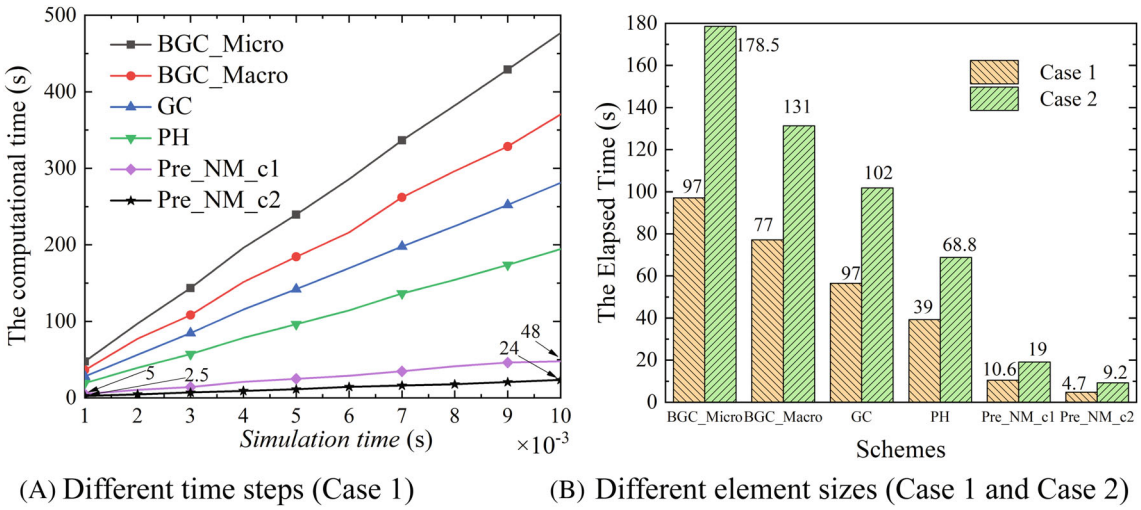

(A) Different time steps (Case 1) (B) Different element sizes (Case 1 and Case 2)

FIGURE 14 Computational time of various methods with parameter combination 1 (Pre_NM_c1: $\gamma_A = \gamma_B = 1/2$ and $\beta_A = \beta_B = 1/4$) parameter combination 2 (Pre_NM_c2: $\gamma_A = \gamma_B = 1/2$ and $\beta_A = \beta_B = 1/6$)

subdomains; computational information exchange between subdomains is only conducted at the system time step; and the time-consuming border programme is not required in the computation. Therefore, the efficiency of the proposed method is improved significantly compared to the existing MMTS methods. In addition, compared with the computational time using the implicit scheme, the explicit schemes of the proposed method can largely reduce the computational time.

7 | CONCLUSIONS

In this study, an efficient partitioned/combined computational method with energy conservation property was proposed to solve dynamic systems with multiple temporal and element scales (i.e., multi-subdomains ≥3). Generalized-α integration schemes[32] with desirable algorithmic damping were extended and incorporated into the proposed method to filter spurious high-frequency vibration content effectively and retain the second-order accuracy simultaneously. The theoretical demonstration was given in detail. Two representative examples were used to demonstrate the accuracy, energy properties, and efficiency of the proposed method.

The novelty of this paper lies in (1) decomposing an entire computational domain into several independent computational subdomains (≥3), (2) combining several independent substructures with different time steps and integration schemes into an entire computational domain, (3) ensuring the desirable algorithmic damping and accuracy by using the Generalized-α schemes, and (4) improving the computational efficiency significantly and the accuracy. Some of the key contributions to the paper are as follows:

1. Computational information exchange between subdomains or substructures is only conducted at the interfaces of interconnected subdomains and the system time step. Moreover, only once subdomain calculation under link forces and external forces is conducted for each time step compared with other existing methods. Therefore, the computational efficiency is improved significantly.
2. The proposed method has the energy conservation property, but a small part of the system mechanical energy would be transferred into the periodic interface mechanical energy. Therefore, the proposed method features the interface pseudo-energy conservation property.
3. The unconditional stability of the implicit scheme and the high efficiency of the explicit scheme are retained in the solving process of different subdomains due to the independence of all subdomains. Generalized-α schemes with desirable algorithmic damping can be employed to filter high-frequency spurious vibration content and ensure the second-order accuracy.

The developed method will be extended to the calculation of subdomains with crossing interfaces and the nonlinear computation in further research.

ACKNOWLEDGMENTS

The study has been supported by the Young Scientists Fund of the National Natural Science Foundation of China (grant no. 52208212). The support is gratefully acknowledged. The opinions and conclusions presented in this paper are those of the authors and do not necessarily reflect the views of the sponsoring organizations.

DATA AVAILABILITY STATEMENT

Data openly available in a public repository that issues datasets with DOIs/researchgate.

ORCID

You Dong https://orcid.org/0000-0002-2499-0999

REFERENCES

1. Yuan P, Li D, Cai CS, Xu G. Time integration method with high accuracy and efficiency for structural dynamic analysis. *J Eng Mech*. 2019;145(3):4019008.
2. Yuan P, Li D, Cai CS, Xu G. A novel decoupling dynamic method with third-order accuracy and controllable dissipation. *Comput. Struct.* 2021;249:106512.
3. Bathe K-J. *Finite element procedures*. Klaus-Jurgen Bathe; 2006.

4. Hughes TJR, Pister KS, Taylor RL. Implicit-explicit finite elements in nonlinear transient analysis. *Comput Methods Appl Mech Eng*. 1979;17:159-182.
5. Smolinski P, Belytschko T, Neal M. Multi-time-step integration using nodal partitioning. *Int J Numer Methods Eng*. 1988;26(2):349-359.
6. Kwak J, Chun T, Shin S, Bauchau OA. Domain decomposition approach to flexible multibody dynamics simulation. *Comput Mech*. 2014;53(1):147-158.
7. Kim W, Lee JH. An improved explicit time integration method for linear and nonlinear structural dynamics. *Comput Struct*. 2018;206:42-53.
8. Park KC. Partitioned transient analysis procedures for coupled-field problems: stability analysis. *J. Appl. Mech*. 1980;47(2):370-376.
9. Farhat C, Roux F-X. A method of finite element tearing and interconnecting and its parallel solution algorithm. *Int J Numer Methods Eng*. 1991;32(6):1205-1227.
10. Farhat C, Crivelli L, Roux F-X. A transient FETI methodology for large-scale parallel implicit computations in structural mechanics. *Int J Numer Methods Eng*. 1994;37(11):1945-1975.
11. Farhat C, Crivelli L, Géradin M. Implicit time integration of a class of constrained hybrid formulations—part I: spectral stability theory. *Comput Methods Appl Mech Eng*. 1995;125(1–4):71-107.
12. Gravouil A, Combescure A. Multi-time-step explicit—implicit method for non-linear structural dynamics. *Int J Numer Methods Eng*. 2001;50(1):199-225.
13. Mahjoubi N, Gravouil A, Combescure A, Greffet N. A monolithic energy conserving method to couple heterogeneous time integrators with incompatible time steps in structural dynamics. *Comput Methods Appl Mech Eng*. 2011;200(9–12):1069-1086.
14. Brun M, Batti A, Limam A, Combescure A. Implicit/explicit multi-time step co-computations for predicting reinforced concrete structure response under earthquake loading. *Soil Dyn Earthq Eng*. 2012;33(1):19-37.
15. Brun M, Batti A, Limam A, Gravouil A. Explicit/implicit multi-time step co-computations for blast analyses on a reinforced concrete frame structure. *Finite Elem Anal Des*. 2012;52:41-59.
16. Prakash A, Hjelmstad KD. A FETI-based multi-time-step coupling method for Newmark schemes in structural dynamics. *Int J Numer Methods Eng*. 2004;61(13):2183-2204.
17. Fekak F-E, Brun M, Gravouil A, Depale B. A new heterogeneous asynchronous explicit—implicit time integrator for nonsmooth dynamics. *Comput. Mech.* 2017;60(1):1-21.
18. Yu K. A new family of generalized-α time integration algorithms without overshoot for structural dynamics. *Earthq Eng Struct Dyn*. 2008;37(12):1389-1409.
19. Prakash A, Taciroglu E, Hjelmstad KD. Computationally efficient multi-time-step method for partitioned time integration of highly nonlinear structural dynamics. *Comput. Struct.* 2014;133:51-63.
20. Gravouil A, Combescure A, Brun M. Heterogeneous asynchronous time integrators for computational structural dynamics. *Int J Numer Methods Eng*. 2015;102(3–4):202-232.
21. Brun M, Gravouil A, Combescure A, Limam A. Two FETI-based heterogeneous time step coupling methods for Newmark and α-schemes derived from the energy method. *Comput Methods Appl Mech Eng*. 2015;283:130-176.
22. Jamal MH, Prakash A, Kulkarni M. Exploiting semantics of temporal multi-scale methods to optimize multi-level mesh partitioning. *Int J Numer Methods Eng*. 2017;112(1):58-85.
23. Marzouk YM, Ghoniem AF. K-means clustering for optimal partitioning and dynamic load balancing of parallel hierarchical N-body simulations. *J Comput Phys*. 2005;207(2):493-528.
24. Yago D, Cante J, Lloberas-Valls O, Oliver J. Topology optimization methods for 3D structural problems: a comparative study. *Arch Comput Methods Eng*. 2021;29:1-43.
25. Yuan P, Dong Y. High-efficient decoupling method for coupling systems with multiple subdomains and time steps. *Mech. Syst. Signal Process.* 2022;163:108159.
26. Yuan P, Li D, Cai CS, Xu G. An efficient decoupling dynamic algorithm for coupled multi-spring-systems. *Comput. Struct.* 2018;209:44-56.
27. Franklin SR, Seshaiyer P, Smith PW. A computational methodology to study coupled physical processes over partitioned domains. *App Math Model*. 2007;31(3):632-646.
28. Abhinav S, Manohar CS. Substructuring tools for probabilistic analysis of instrumented nonlinear moving oscillator—beam systems. *App Math Model*. 2017;42:600-617.
29. Chatterjee T, Adhikari S, Friswell MI. Uncertainty propagation in dynamic sub-structuring by model reduction integrated domain decomposition. *Comput Methods Appl Mech Eng*. 2020;366:113060.
30. De Salvo V, Muscolino G, Palmeri A. A substructure approach tailored to the dynamic analysis of multi-span continuous beams under moving loads. *J Sound Vib*. 2010;329(15):3101-3120.
31. Abbiati G, La Salandra V, Bursi OS, Caracoglia L. A composite experimental dynamic substructuring method based on partitioned algorithms and localized Lagrange multipliers. *Mech Syst Signal Process*. 2018;100:85-112.
32. Krenk S. Energy conservation in Newmark based time integration algorithms. *Comput Methods Appl Mech Eng*. 2006;195(44–47):6110-6124.
33. Li J, Yu K. Development of composite sub-step explicit dissipative algorithms with truly self-starting property. *Nonlinear Dyn*. 2021;103(2):1911-1936.
34. Flores EIS, DiazDelaO FA, Ajaj RM, Friswell MI, Fernando GF. Mathematical modelling of the stochastic mechanical properties of wood and its extensibility at small scales. *App Math Model*. 2014;38(15–16):3958-3967.

35. Li J, Yu K, Li X. An identical second-order single step explicit integration algorithm with dissipation control for structural dynamics. *Int J Numer Methods Eng*. 2021;122(4):1089-1132.
36. Wei Liu XT, Ye T, Yuan P, Beer M. An explicit integration method with third-order accuracy for linear and nonlinear dynamic systems. *Eng Struct*. 2023;274:115013.

How to cite this article: Yuan P, Adhikari S, Dong Y. A partitioned combined computational method for multi-scale dynamic systems. *Int J Numer Methods Eng*. 2023;124(16):3494-3523. doi: 10.1002/nme.7256

APPENDIX A

TABLE A1 Implementation flowchart of Pre_NM

(1) Calculate matrices and parameters of all subdomains
$\boldsymbol{K}^k, \boldsymbol{M}^k, \gamma^k, \beta^k, \Delta h^k, \boldsymbol{K}^{*k}, \left(\boldsymbol{L}_l^{k\cdot jT} j = (1, \ldots, S_k)\right)$ (see Equation 12)
(2) Given initial conditions and condensed matrix
$\boldsymbol{u}_{t_0}^k, \boldsymbol{v}_{t_0}^k, \overline{\boldsymbol{V}}_{K\cdot J}, \boldsymbol{H}_{K\cdot J}, \boldsymbol{H}_{K\cdot f1}, \boldsymbol{H}_{J\cdot f1}$, (see Equation (37))
(3) Calculate link forces at the system time step
$\overline{\boldsymbol{V}}_{K\cdot J}$ (see Equation (36))
(4) Calculate the responses of all subdomains
$\mathbb{K}_*^k \Delta \mathbb{U}_{t_k}^k = \mathbb{F}_{t_k}^k - \mathbb{L}_k^T \Delta \mathfrak{R}_{t_k}^k \qquad \forall t_k \in \{1, m_k\}$ (see Equation (42))
(5) Return to (3) for the next step or stop